THE ASTROPHYSICAL JOURNAL, 289:81–104, 1985 February 1

ROTATION VELOCITIES OF 16 Sa GALAXIES AND A COMPARISON OF Sa, Sb, AND Sc ROTATION PROPERTIES

VERA C. RUBIN[1,2,3]
Department of Terrestrial Magnetism, Carnegie Institution of Washington
DAVID BURSTEIN[4]
Arizona State University, Tempe
AND
W. KENT FORD, JR.,[2,3,5] AND NORBERT THONNARD
Department of Terrestrial Magnetism, Carnegie Institution of Washington
Received 1984 May 29; accepted 1984 August 10

ABSTRACT

Rotational velocities are presented for 16 Sa galaxies; for 11 of these, velocities extend to beyond 66% of R_{25}. The Sa rotation curves show the same progression as do the Sb and Sc rotation curves, from low central gradient, low rotational velocity for Sa's of low luminosity, to high central gradient, high rotational velocity for Sa's of high luminosity. There is a marked similarity of form (but not of amplitude) of rotation curves for galaxies with morphologies as different as large-bulged Sa's and small-bulged Sc's. This suggests that the form of the gravitational potential is not strongly correlated with the form of the optical luminosity distribution.

Parameters for the Sa galaxies are compared with those for Sb and Sc galaxies. The maximum rotation velocities for Sa galaxies are higher than those of Sb and Sc galaxies of equivalent blue or infrared magnitude. Median values of V_{max} decrease from 299 to 222 to 175 km s^{-1} for the Sa, Sb, and Sc samples, respectively. The Tully-Fisher correlation of luminosity with V_{max} has slopes near 10 for Sa, Sb, and Sc galaxies separately, but with zero-point displacements. An Sa galaxy with V_{max} equal to that of an Sc is 2 mag fainter in the blue, and over 1 mag fainter in the infrared H band, than the Sc. Thus the differences between the properties of the galaxies in our sample and those drawn from the H I–selected samples of Aaronson *et al.* persist even when H magnitudes are used in the correlations. We suggest that selection effects in choosing the galaxies are the probable cause.

Subject headings: galaxies: internal motions — galaxies: structure

I. INTRODUCTION

For the past several years, we have been studying the dynamical properties of field spiral galaxies. Our aim is twofold: to deduce the systematic properties of galaxy dynamics and mass distribution among galaxies with a wide range of luminosity within a Hubble type and with a wide range of Hubble types; and to relate the dynamical parameters to other galaxy properties as one step in the effort to understand the formation and evolution of spiral galaxies. As a continuation of this program we present observations of 16 Sa galaxies. Previous papers have discussed the rotational properties of 21 Sc galaxies (Rubin, Ford, and Thonnard 1980, hereafter Paper I), 23 Sb galaxies (Rubin *et al.* 1982, hereafter Paper II), and the mass distribution for the Sc galaxies (Burstein *et al.* 1982, hereafter Paper III).

The Sa's chosen for study are (*a*) classified Sa by Sandage and Tammann (1981), or by de Vaucouleurs, de Vaucouleurs, and Corwin (1976); (*b*) not strongly barred; (*c*) of relatively high inclination as judged from the axial ratio of the disk (not from the major-to-minor axis ratio, for the minor axis often measures principally the bulge); (*d*) distributed over the largest range of luminosity which we could identify; and (*e*) smaller than a few arc minutes in diameter. In general, we favor large-bulged systems to ensure a significantly different morphology from that of the Sb's, but the available pool is limited, and we relax this condition as necessary. The Sa's we have picked for study are drawn from one end of a continuous distribution which encompasses Sb's and Sc's as well. Their properties are not discontinuous from the later types. In general, the Sa's are not as isolated as are the Sb and Sc galaxies but often occur in loose groups containing a few galaxies.

The rotation curve data for the Sa sample are presented in a fashion analogous to that used for the Sb and Sc samples. The observations are discussed in § II, and rotation velocities for the entire Sa, Sb, and Sc set are presented together in Appendix A. For the Sa set, rotational velocities for each half of the major axis are shown superposed, in order to illustrate the degree of symmetry within each galaxy. Rotation properties are discussed in § III. Rather than analyze the properties of the Sa's alone, we present a general discussion of the systematic variation of properties among Sa, Sb, and Sc galaxies in § IV. For these 54 galaxies, a comprehensive study of the properties of their mass distributions and the relation to their nonluminous halos will be given elsewhere (Burstein and Rubin 1985).

Infrared H magnitudes are now available for the galaxies in our sample (Aaronson 1983). We show in § V that differences

[1] Visiting Astronomer, Cerro Tololo Inter-American Observatory, National Optical Astronomy Observatories, supported by the National Science Foundation under contract AST 78-27879.
[2] Visiting Astronomer, Kitt Peak National Observatory, National Optical Astronomy Observatories, which is operated by the Association of Universities for Research in Astronomy, Inc., under contract with the National Science Foundation.
[3] Adjunct Staff Member, Mount Wilson and Las Campanas Observatories.
[4] Adjunct Assistant Astronomer, Steward Observatory.
[5] Visiting Astronomer, Lowell Observatory.

between the galaxies in our sample and those drawn from H I–selected samples (e.g., Aaronson *et al.* 1982; Aaronson and Mould 1983; de Vaucouleurs *et al.* 1982; Tully, Mould, and Aronson 1982) persist even when infrared magnitudes are used in the correlations. The probable cause of this difference, selection effects in choosing the samples, is also discussed.

II. BASIC DATA FOR THE Sa GALAXIES

a) The Observations

We have used the 4 m telescopes at Kitt Peak and Cerro Tololo observatories, and the 2.5 m telescope on Las Campanas to obtain image-tube spectra centered near Hα for the program galaxies. Spectrograms of high dispersion and at high spatial scale were obtained with the slit aligned along the major axis. Spectrograms along the minor (or other) axis were obtained for seven of the galaxies. Dispersions and scales are 25 Å mm^{-1} (occasionally 50 Å mm^{-1}) and 25″ mm^{-1} for the 4 m spectra, and 63 Å mm^{-1} and 52″ mm^{-1} for the 2.5 m spectra. All three spectrographs incorporate an RCA C33063 Carnegie image tube, and the final phosphor is imaged into IIIa-J plates which have been baked in forming gas and preflashed. Exposure times are generally 2 or 3 hr for the major axis plates.

Galaxies included in the study are listed in Table 1. Reproductions of the galaxies and the major axis spectra are shown in Figure 1 (Plates 2 and 3). Detailed results for NGC 4378 have appeared earlier (Rubin *et al.* 1978). Our observations of NGC 4594 (the Sombrero) extend with the same equipment the work of Schweizer (1978).

Spectra were measured on a Mann two-dimensional measuring machine at DTM. Hα and [N II] lines were routinely

TABLE 1

PARAMETERS FOR Sa GALAXIES

NGC IC UGC (1)	Class RSA (2)	$V_\odot$ (km s^{-1}) (3)	V_{LG} (km s^{-1}) (4)	Distance (Mpc) (5)	Observed Position Angles (degrees) (6)	Line of Nodes (degrees) (7)	Inclination (degrees) (8)	R_{25} (arcmin) (9)	$R_{25}^{i,b}$ (kpc) (10)	$R_f/R_{25}^{i,b}$ (11)
N1024	PSAR2	+3520 ± 15	+3590	71.7(g)	149, 155	155	68	2.34	50.5	1.02
N1357	Sa(s)	+2038 ± 15	+1967	39.3	85	85	45	1.23	14.2	0.73
N2639	Sa	+3193 ± 10	+3238	66.5(g)	135, 140	135	65	1.00	19.3	0.75
N2775	Sa(r)	+1355 ± 15	+1185	24.3(g)	154.9	163	44	2.23	15.9	0.67
N2844	Sa:(r)	+1498 ± 15	+1491	29.8	12.8	13	74	0.95	7.9	0.85
N3898	Sa I	+1165 ± 15	+1264	23.1(g)	107	109.5	67	2.18	14.1	0.96
N4378	Sa(s)	+2544 ± 15	+2431	48.6	58, 7.5, 0	164(d)	35	1.66	22.5	0.98
N4594	Sa+/Sb−	+1092 ± 20	+ 927	18.5	87, 90	87	84	4.46	23.5	0.69
N4698	Sa	+1014 ± 10	+ 932	20(g)	171	170	70	2.13	11.9	0.69
U10205	Sa	+6581 ± 15	+6734	135	42, 132	132(d)	84	0.85	40.1	0.68
I724	Sa	+5965 ± 10	+5844	117	59.9	60	55	1.25	48.3	0.76
N3281	Sa	+3396 ± 20	+3115	62.3	46, 136, 138	138(d)	69	1.66	31.4	0.35
N3593	Sa pec	+ 637 ± 15	+ 520	12.4(g)	92	92	67	2.88	9.8	0.26
N4419	SB ab:	− 198 ± 15	− 266	20(g)	130, 132	132	71	1.69	9.3	0.48
N4845	Sa	+1101 ± 20	+ 998	20	78	78	72	2.51	13.5	0.52
N6314	SaS1*	+6642 ± 15	+6822	138(g)	175	175	70:	0.89	36.1	0.53

NOTES.—Col. (2), classification from RSA (Sandage and Tammann 1981); except NGC 1024, NGC 6314 from RC2 (de Vaucouleurs, de Vaucouleurs, and Corwin 1976); IC 724, UGC 10205 from UGC (Nilson 1973). Col. (3), night-sky OH lines used for velocity standards for NGC 4594; wavelengths from Brault and Hubbard 1981. All other spectra use comparison neon lines. Velocity is center of symmetry of rotation curves. Col. (4), $V_{LG} = V_\odot + 300 \sin l \cos b$. Col. (5), distance = V_{LG}/H_0 ($H_0 = 50$ km s^{-1} Mpc^{-1}); those with (g) are group distances. See notes to individual galaxies below. Col. (7), measured from POSS or UGC, except NGC 2775 and NGC 3898 from Boroson 1981. The notation (d) indicates line of nodes calculated from velocities in several position angles. Col. (8), calculated from parameters of disk measured from available plate material or POSS, except NGC 2775 and NGC 3898 from Boroson 1981. Col. (9), from RC2 or UGC. Col. (10), $\log R_{25}^{i,b} = \log R_{25} - 0.07 \log a/b - \log(1 - \Delta m_b/3.35)$ (Papers II and III). Col. (11), $R_{farthest}$ is R of most distant velocity measure.

NOTES FOR INDIVIDUAL GALAXIES

NGC 1024.—Arp 333. Sa galaxy with distant faint outer arms which form pseudo-ring. Velocities of wisp (superposed on star on ring, which leads to its inclusion in the Arp 1966 atlas) are lower than V_{max}, producing falling rotation curve. However, there is no evidence that wisp motions are circular velocities. Star on ring has velocity near zero, as measured from Hα absorption. Pair at 7′ with NGC 1029 ($V_{LG} = 3583$ km s^{-1}).

NGC 2639.—In loose group with NGC 2684 ($V_{LG} = 3373$ km s^{-1}) and UGC 4544 ($V_{LG} = 3360$ km s^{-1}).

NGC 2775.—Pictured in *Hubble Atlas* (Sandage 1961). In loose group with NGC 2777 ($V_{LG} = 1317$ km s^{-1} at 11′) and UGC 4797 ($V_{LG} = 1140$ km s^{-1}).

NGC 2844.—Probable pair with NGC 2852 (no velocity) at 5′.

NGC 3898.—Pictured in *Hubble Atlas* (Sandage 1961). Member de Vaucouleurs 1975 G34; mean of 30 velocities gives $V_{LG} = 1154 \pm 43$ km s^{-1}.

NGC 4378.—Beyond Virgo Cluster. See Rubin *et al.* 1978 for details.

NGC 4594.—Sombrero galaxy. Spectra in several position angles are presently being studied, so rotation curve here is preliminary. Inner velocity peak at $r = 400$ pc, observed on 20 minute exposure, is hidden in bulge continuum on 180 minute exposure in Fig. 1.

NGC 4698.—In Virgo Cluster.

UGC 10205.—Prominent bulge seen through absorbing disk; resembles Sombrero galaxy. Curious velocity structure confirmed on several plates. On SE major axis, three velocity systems are observed within 10 kpc of the nucleus. Minor axis velocities appear normal on weak minor axis spectrum.

NGC 3281.—Attractive symmetrical spiral with extended asymmetrical plume to SE. Emission broad and intense in nucleus, weak beyond. In loose group; no other velocities.

NGC 4419.—Central velocity negative; assumed to be in Virgo Cluster. Rotation velocity extends only to $0.48R_{25}$, even with repeated attempts and exposure of 201 minutes. From statistics of other Sa's, velocity of 181 km s^{-1} at $0.48R_{25}$ extrapolates to 205 km s^{-1} at R_{25}. From relation of V_{max} and M_B (Fig. 9*a*), this implies a distance of 15.3 Mpc.

NGC 4845.—Not in Virgo Cluster. Strong nuclear emission, weak beyond. Not detected at 21 cm.

NGC 6314.—Pair with NGC 6315 ($V_{LG} = 6956$ km s^{-1}) at 3′.2.

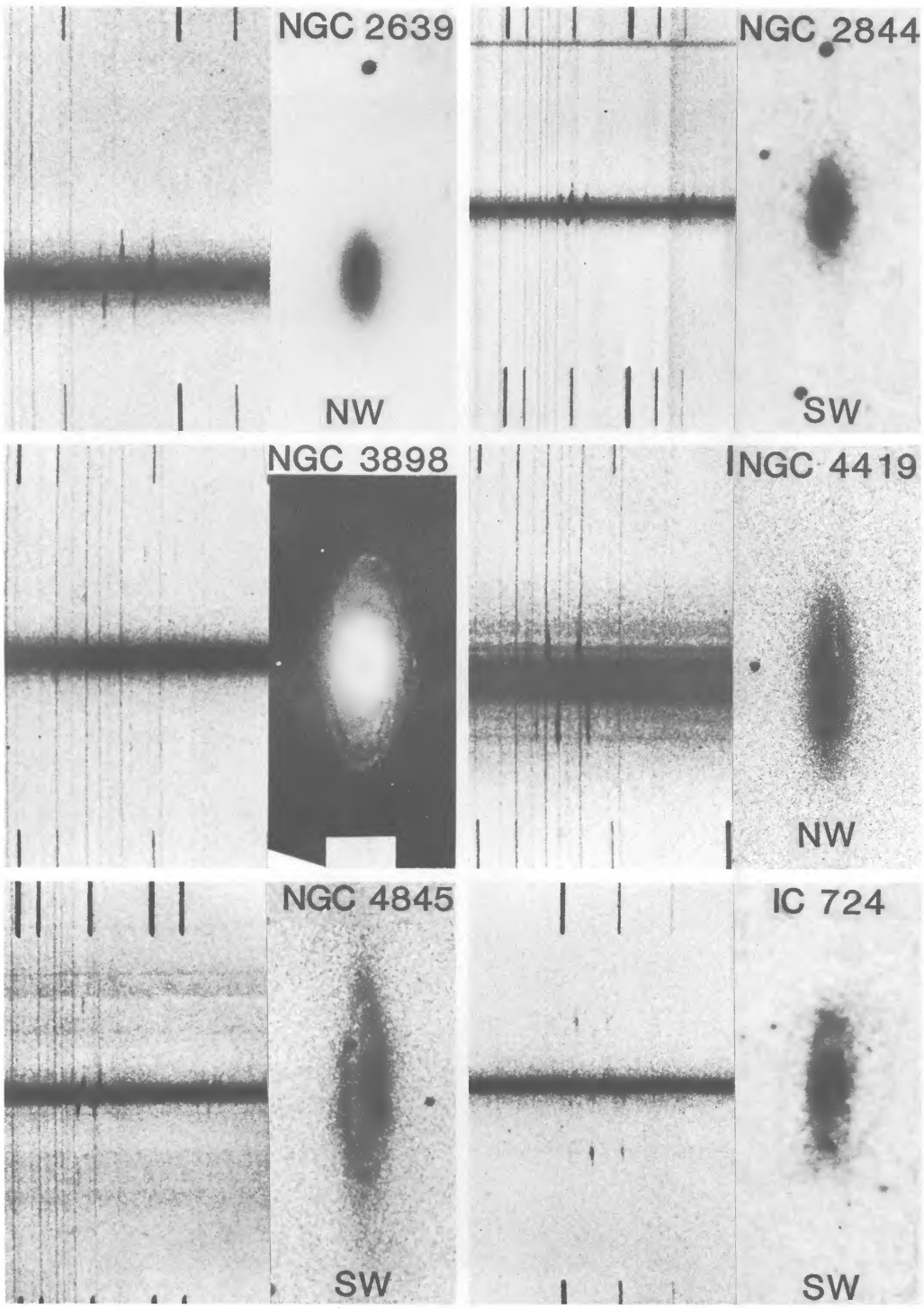

FIG. 1*a*

FIG. 1.—Reproductions of spectrograms and direct plates for 12 of 16 Sa galaxies in study. All spectra and galaxies are printed here to approximately the same angular scale. On each spectrum, red is to the right. On spectra of highest dispersion (25 Å mm^{-1}), the strongest line is Hα, flanked by two [N II] lines. On spectra at lower dispersion (50 Å mm^{-1}: NGC 2844, 3593, and 4845), the [S II] doublet is seen redward of Hα and [N II]. The weak undistorted lines crossing the spectra are night-sky OH lines. The spectra were taken with the KPNO or CTIO 4 m telescope plus Ritchey-Chrétien spectrograph plus Carnegie image tube on baked and preflashed IIIa-J plates. Exposures are generally 2–3 hr. Photographs of NGC 1024, 2844, 3593, and IC 724 are copies of Palomar Observatory Sky Survey plates (copyright National Geographic Society–Palomar Observatory); NGC 4419 and 4845 are from Palomar Schmidt plates (103a-O + GG13, 30 minutes); UGC 10205 is from a Palomar Schmidt plate (IIIa-F + Wr25); NGC 3281 is copied from an ESO-SRC red film; NGC 2775 and 3898 are copied from the *Hubble Atlas*, courtesy of A. Sandage; NGC 4594 is a copy of a 30 minute CTIO 4 m prime-focus plate, UG5 filter, baked 103a-O, courtesy of F. Schweizer; and NGC 2639 comes from a 20 minute exposure, Carneigie image-tube plus RG23 filter plus baked IIIa-J plate, Lowell Observatory 42 inch (1.1 m) telescope.

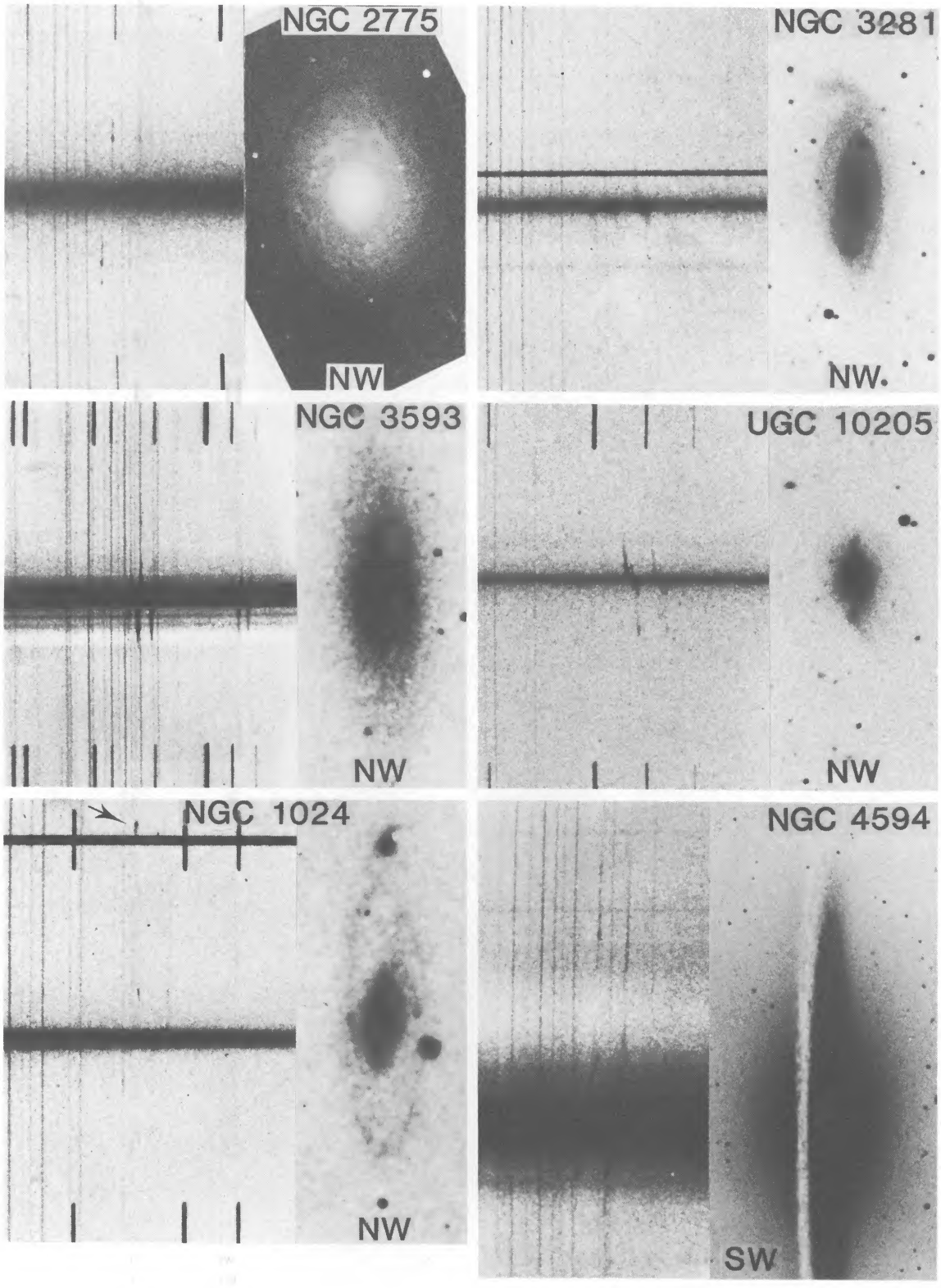

FIG. 1*b*

RUBIN *et al.* (*see* page 82)

measured, but [S II] lines were measured only if there was night-sky contamination at Hα or [N II]. For all spectra except those for NGC 4594, neon comparison lines were used to establish the rest frame and distortions. For NGC 4594, OH night-sky lines were used instead. Accurate wavelengths for OH lines come from Brault and Hubbard (1981). Velocities are calculated in the optical convention: $V = cz = c(\lambda - \lambda_0)/\lambda_0$; and rotational velocities include the correction for the relativistic Doppler shift, $1/(1 + z_0)$ (Harrison 1974).

Line emission is generally more difficult to detect in the Sa galaxies than in the Sb and Sc samples. This is not unexpected, in view of the small number of knotty H II regions apparent in the arms of the Sa's. Two very distinct patterns of emission are observed. For some of the Sa's (NGC 1024, 2775, 4378, IC 724) only weak (or no) emission is detected in the region of the bulge, but patchy Hα and [N II] appear in the disk beyond. A second pattern of emission is also seen (NGC 3281, 4845), where strong diffuse nuclear emission decreases in intensity with increasing radial distance in the disk, but with no indication of resolution into knots.

Due to the overall weakness of the emission, we have been less successful in measuring velocities across the optical image in these Sa's than for the Sb and Sc samples. Only for 11 Sa's have we measured velocities over more than 66% of the optical image, i.e., over a few disk scale lengths; for five others we have measured velocities over a smaller fraction of the galaxy. And for five galaxies [NGC 2618, 2769, 3312(pec), 3571, and 4305] we have detected no measurable emission. These five galaxies are not discussed further.

For each galaxy, measured heliocentric velocities on the plane of the sky as a function of angular distance from the nucleus are shown in Figure 2. The center of symmetry of the velocities is adopted as the heliocentric velocity of the galaxy (Table 1, col. [3]).

b) Basic Data

The physical data for the Sa galaxies are given in Table 1; definitions accord with those we have employed for the Sb and Sc samples. The distance for each field galaxy (col. [5]) comes from its central velocity, corrected for the motion of the Sun with respect to the Local Group, $\Delta V = 300 \cos b \sin l$, with $H_0 = 50$ km s^{-1} Mpc^{-1} (col. [4]). There are no significant changes if we adopt a Virgocentric flow model (Schechter 1980) instead. Galaxies in small groups are identified in the notes to Table 1, and distances for these come from the mean velocity of the group. Three galaxies, NGC 4419 ($V_\odot = -198$), NGC 4698 ($V_\odot = +1014$), and NGC 4845 ($V_\odot = +1101$), are assumed to be members of the Virgo Cluster, at an adopted distance of 20 Mpc. But even this distance choice is not significant, for NGC 4419 and 4845 are not included in the correlations we derive below, as their rotational velocities have not been determined to large radii. For the Sa galaxies, central velocities are accurate to about 10 km s^{-1}. Radial velocities for 15 of these Sa galaxies are listed in the Huchra (1984) compilation. The value of the difference, $\langle |\Delta V| \rangle = \langle |V_{\rm Hu} - V_{\rm here}| \rangle$, is 44 km s^{-1} (but this may represent a lower limit, for a few of the Huchra tabulated velocities may come from velocities determined by Rubin). The value $(44^2 - 10^2)^{1/2}$ is close to the 37 km s^{-1} accuracy which Rood (1982) has assigned to the Huchra velocities.

We have ample evidence that the optical velocities of the Rubin *et al.* sample are virtually identical to the 21 cm velocities. For 42 Sa, Sb, and Sc galaxies which we have observed at 21 cm (Thonnard 1982), the mean difference in systemic velocity is $\langle V_{\rm opt} - V_{21} \rangle = -1.5 \pm 3.9$ km s^{-1} (Thonnard 1982). For the 35 Sb and Sc galaxies, the difference between the maximum rotational velocity and one-half the 21 cm profile read at 50% of the peak is $\langle V_{\rm max}({\rm opt} - 21) \rangle = 0.8 \pm 2.0$ km s^{-1}. For the seven Sa galaxies detected at 21 cm (Thonnard, unpublished), only two show a nonzero difference between the optical and 21 cm $V_{\rm max}$. Thus all of the correlations discussed below would be virtually identical if 21 cm velocity widths had been used in place of the maximum optical rotation velocity.

Observed slit position angles are listed in column (6), and the adopted line of nodes is listed in column (7). These are marked (d) if they are determined dynamically from velocities in two or more position angles; otherwise they come from measurements of the Palomar Observatory Sky Survey prints. The inclination (col. [8]) comes from our estimate of the major and minor axes of the *disk* and assumes that the disk is not seriously warped. This assumption should be generally valid over the optical galaxy. We have made every effort not to confuse a large bulge with a minor axis disk measure.

The isophotal radius of the galaxy, R_{25}, the distance where the surface brightness has fallen to 25 B mag arcsec^{-2} (RC2), is listed in column (9). The linear radius, corrected for internal and external extinction, is in column (10). The ratio $R_f/R_{25}^{i,b}$ is given in column (11); R_f is the distance from the nucleus of the farthest measured velocity.

Integral properties derived from the observed quantities are listed in Table 2. Blue magnitudes (col. [3]) come from RC2 when available; otherwise they come from Nilson (1973). Corrections to apparent magnitudes for galactic extinction (col. [4]) come from Burstein and Heiles (1984). Corrections for internal extinction (col. [5]) to face-on magnitudes, $\Delta m_i = 1.90 \log (a/b)$, are similar to those used in Papers II and III. The adopted constant for the internal extinction is that previously used for the Sb and Sc samples, for we detect no significant difference in extinction properties among different Hubble types. Note, however, that the correlations among the integrated parameters are not significantly dependent on extinction models, as most of the galaxies are of similar inclinations. The corrected apparent blue magnitude, $B^{i,b}$, is given in column (6), and the resulting absolute blue magnitude M_B in column (7). Columns (8) and (9) list the velocity at the farthest distance $V(R_f)$ and the maximum observed velocity, $V_{\rm max}$. We use $V_{\rm max}$ as a measure of the rotation velocity in the correlations discussed below. No significant difference would result from using velocities extrapolated out to R_{25}. The absolute infrared luminosity, L_H, has been calculated from values of $H_{-0.5}$ kindly supplied by M. Aaronson. Corrections to $H_{-0.5}$ for internal and external extinction follow the precepts of Burstein (1982).

In an effort to keep the analysis as simple as possible, we model the mass distribution for each galaxy as a sphere; the mass interior to R_{25} is given by $\mathcal{M}(R_{25}) = GR_{25}V^2(R_{25})$ (col. [10]). Unfortunately, analysis of rotation curves reveals no details of the mass distribution interior to R_{25}. If the mass is distributed in a disk rather than a sphere, then the mass interior to R_{25} will be smaller than that calculated for a sphere by amount $2/\pi$. This difference is insignificant for our purpose. For galaxies where V has not been measured as far as R_{25}, V is assumed flat from the final measured value, typically giving a lower limit to $\mathcal{M}(R_{25})$. Columns (11) and (12) list the ratios of mass within the optical radius to the blue and to the infrared luminosities, respectively.

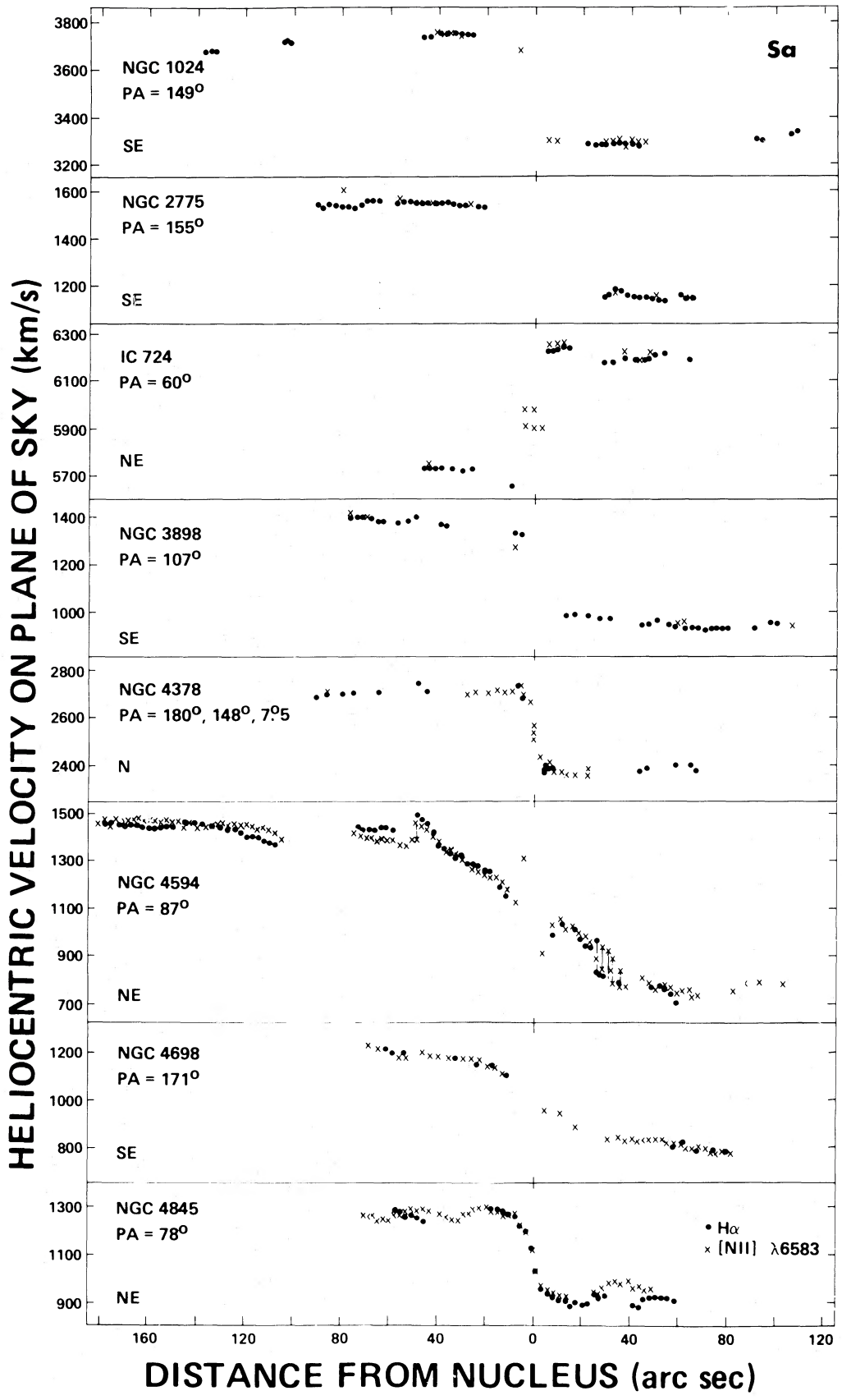

FIG. 2*a*

FIG. 2.—Heliocentric line-of-sight velocities for 16 Sa galaxies as a function of angular distance from the nucleus. Only measures from Hα and [N II] λ6584 are plotted.

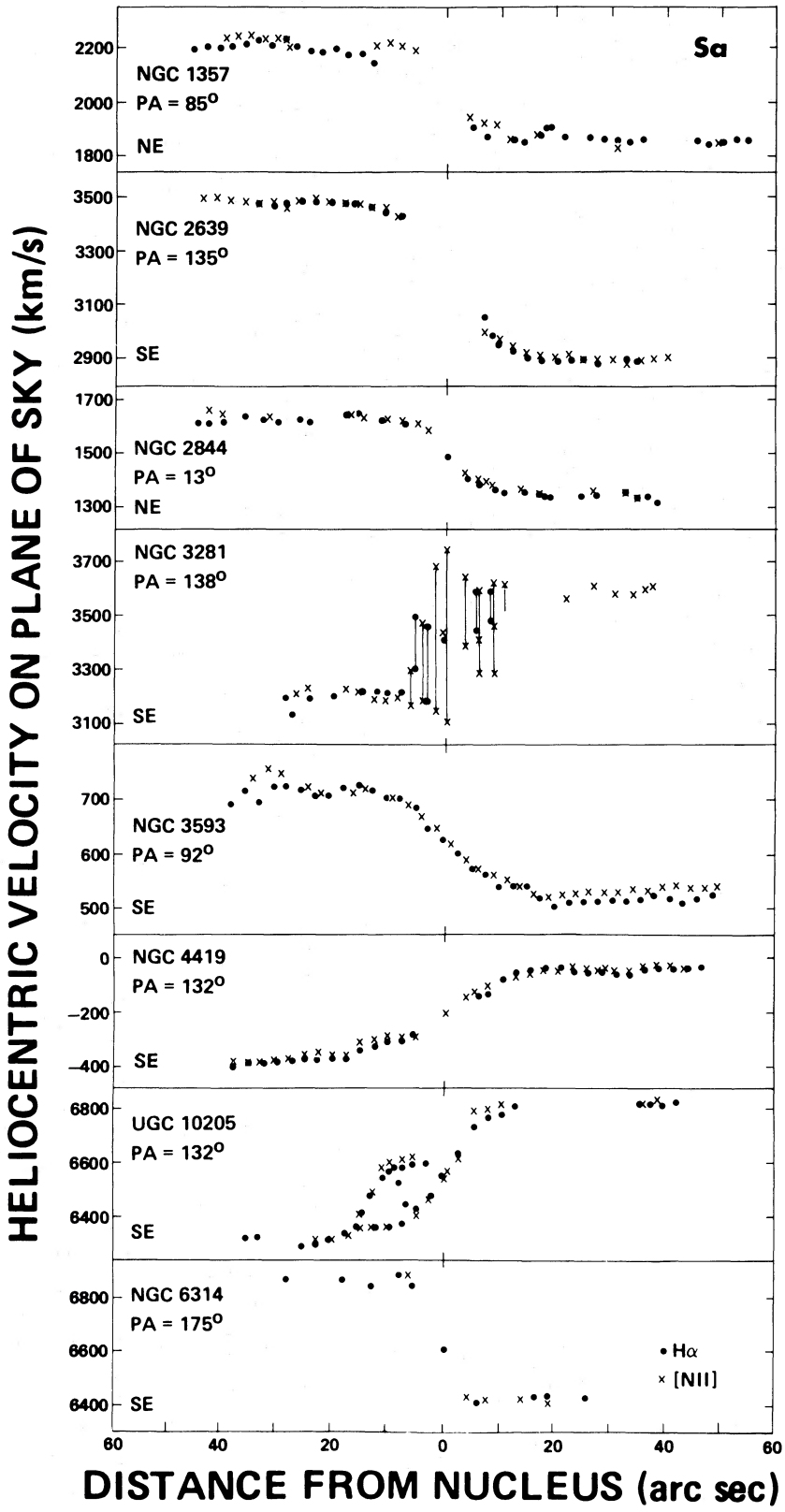

FIG. 2*b*

TABLE 2

ADDITIONAL PARAMETERS FOR Sa GALAXIES

NGC IC UGC (1)	Distance (Mpc) (2)	B_T (mag) (3)	Δm_b (mag) (4)	Δm_i (mag) (5)	$B^{i,b}$ (mag) (6)	M_B (mag) (7)	$V(R_f)$ (km s^{-1}) (8)	V_{max} (km s^{-1}) (9)	$\mathcal{M}(R_{25})$ (10^{10} $M_\odot$) (10)	$\mathcal{M}(R_{25})/L_B$ (11)	$\mathcal{M}(R_{25})/L_H$ (12)
N1024	71.7	13.8	0.30	0.72	12.8	−21.5	140	272	23.5	3.8	0.6
N1357	39.3	12.60	0.09	0.27	12.24	−20.7	256	269	21.8	7.4	...
N2639	66.5	12.65	0.09	0.34	12.22	−21.9	324	324	46.9	5.2	1.5
N2775	24.3	11.20	0.09	0.19	10.92	−21.0	273	299	27.8	7.1	2.0
N2844	29.8	13.65	0	0.55	13.10	−19.3	163	163	4.87	6.0	2.4
N3898	23.1	11.7	0	0.44	11.3	−20.5	269	269	23.8	9.6	2.9
N4378	48.6	12.28	0	0.06	12.22	−21.2	283	322	41.8	8.9	...
N4594	18.5	9.27	0.11	0.65	8.51	−22.8	367	367	73.6	3.6	1.2
N4698	20.	11.39	0	0.46	10.93	−20.6	248	248	17.0	6.3	2.9
U10205	135.	14.4	0.05	0.52	13.8	−21.9	243	275	55.1	6.2	1.4
I724	117.	13.8	0.02	0.76	13.0	−22.3	286	374	91.9	7.1	2.1
N3281	62.3	12.62	0.28	0.51	11.83	−22.1	229	...	...	...	...
N3593	12.4	11.7	0	0.70	11.0	−19.5	108	...	...	...	...
N4419	20.	11.95	0.05	0.82	11.08	−20.4	181	...	...	...	...
N4845	20.	12.17	0.01	0.95	11.2	−20.3	175	...	...	...	...
N6314	138.	13.85	0.20	0.55	13.10	−22.6	229	...	...	...	...

NOTE.—Col. (2), from Table 1. Col. (3), RC2, except N1024, I724, N3898, U10205 from UGC. Col. (4), from Burstein and Heiles 1984. Col. (5), $\Delta m_i = 1.9 \log (a/b)$ (Papers II and III).

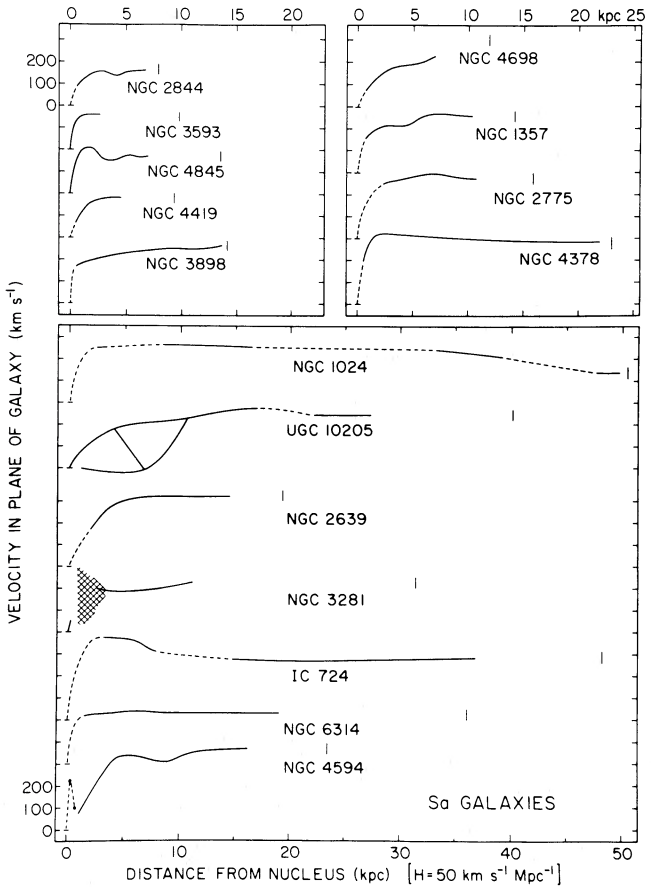

FIG. 3.—Rotation curves for 16 Sa galaxies, showing mean velocity in the plane of the galaxy as a function of linear radius, arranged from low luminosity (*top*) to high luminosity (*bottom*). Small vertical marks indicate the location of R_{25}, the isophote of 25th magnitude arcsec^{-2}. For NGC 1024, most distant velocities come from outer ring; UGC 10205 exhibits triple-valued velocities on one side of the major axis; NGC 3281 bulge emission is diffuse and broad, as indicated by cross-hatching; NGC 4594 has inner velocity peak which is just resolved.

III. THE ROTATION CURVES OF Sa GALAXIES, AND COMPARISON OF HUBBLE TYPES

As in our previous analyses, we assume that the emission lines in Sa disks arise from gas which is moving in planar circular orbits about the center of each galaxy. These circular velocities are derived from the measured velocities, the adopted major axis, and the adopted inclination. The rotation curve is formed by maximizing (by eye) the symmetry of velocities on both sides of the major axis, with some smoothing. Rotation curves for the Sa galaxies, plotted all to the same linear scale, are shown in Figure 3. In practice, velocities are generally fairly symmetrical about the central velocities, as can be seen from Figure 12.

The Sa rotation curves show the same progression with increasing luminosity as do the Sb and Sc rotation curves: from low central gradient, low rotational velocity for galaxies of low luminosity, to high central gradient, high rotational velocity for Sa's of high luminosity. As a class, the forms of the rotation curves for the Sa galaxies match fairly well those for the Sb and Sc galaxies, with the Sa's showing only marginally more individuality. Six Sa's have rotation curves which show significant deviations from a monotonically rising (or flat) rotation curve, while only two have large velocity gradients near their centers. By comparison, a similar percentage of Sb's and Sc's (six and eight galaxies, respectively) have rotation curves which deviate from monotonically rising. However, many of the more luminous Sb and Sc galaxies have large velocity gradients near their centers. For galaxies at each luminosity, however, rotational velocities are higher in Sa's than in Sb's or Sc's.

We have exploited this smooth progression of rotation curve properties to form synthetic rotation curves for Sa, Sb, and Sc galaxies (Fig. 4). These synthetic curves show the forms of rotation curves as a function of luminosity, within a Hubble type. The details of producing these curves are described in Appendix B.

We first discuss the Sa synthetic rotation curves. Sa's of the lowest luminosity ($M_B = -18$) generally reach their maximum

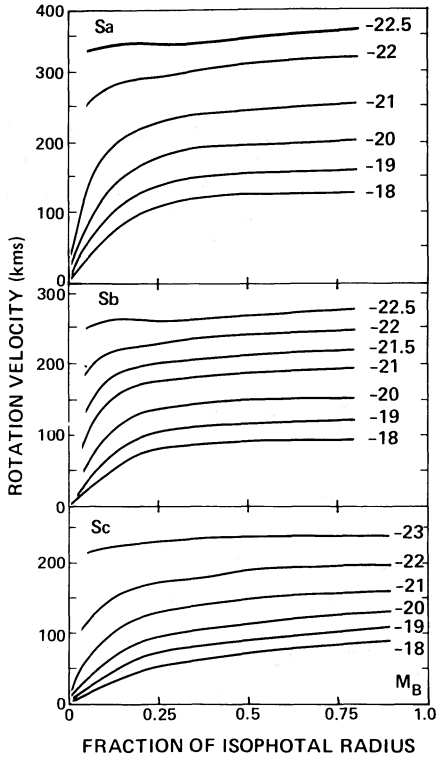

FIG. 4.—Synthetic rotation curves showing average smoothed rotation velocity as a function of fraction of isophotal radius, R_{25}, for (*top*) Sa galaxies of successive luminosities, (*middle*) Sb galaxies, and (*bottom*) Sc galaxies. The procedure for synthesizing these curves is described in Appendix B.

rotational velocity, $V_{max} = 100$ km s^{-1}, in a large fraction (often 70%–80%) of their isophotal radius, R_{25}. In contrast, Sa's of highest luminosity ($M_B = -22.5$) often reach a velocity close to their maximum rotation velocity, $V_{max} = 350$ km s^{-1}, in a small fraction ($\sim 10\%$) of their isophotal radius. But because low-luminosity galaxies are small, and high-luminosity galaxies are large, galaxies of all luminosities reach velocities near their maximum rotational velocities within a few kpc of the nucleus.

This same sequence of synthetic Sa rotation curves is plotted on a *linear* radial scale in Figure 5; the smooth variation from one curve to the next remains obvious. We have observed no rotation curves for (noninteracting) galaxies which deviate sharply from these. There is not, for example, a rotation curve for a high-luminosity galaxy which rises very gradually across the galaxy, or which is flat at a low velocity; and it is rare to observe a rotation curve for a low-luminosity spiral which is flat over most of the galaxy.

It is also remarkable that the forms of the synthetic rotation curves are very similar for all of the Hubble types, regardless of morphology (Fig. 4). This similarity is emphasized in Figure 6, where we plot the rotation curves for an Sa, an Sb, and an Sc galaxy, whose bulge-to-disk ratios range from 4.0 to 0.1 (Whitmore 1984). The similar shapes of the rotation curves reflect none of the marked structural differences which led to their different morphological classifications. Lest we overemphasize this similarity, we point out that the synthetic rotation curves for the Sa, Sb, and Sc galaxies do have differences in form; we have not yet established whether or not these differences are significant. Moreover, there are individual characteristics superposed on the general form, as shown by the rotation curves for the Sa galaxies (Fig. 12).

The apparent similarity and relative simplicity in the forms of the rotation curves of the Sa, Sb, and Sc galaxies are surprising, as these Sa's were chosen to be bulge-dominated. This similarity is added evidence that the optical luminosity does not map the gravitational potential *anywhere* within the optical galaxy. As we discuss below in connection with $\mathcal{M}/L$ ratios, the nonluminous component must contribute to the overall gravitational potential at all radii. These observations suggest that the forms of the distributions of mass within the more extended halos are similar except for radial and/or density scale factors, independent of the morphology of the optical galaxy.

IV. COMPARATIVE INTEGRATED PROPERTIES OF THE Sa, Sb, AND Sc PROGRAM GALAXIES

In this section, we compare integral properties of Sa, Sb, and Sc galaxies which we have studied. Rotational velocities for the Sa, Sb (Paper II), and Sc (Papers I and III) galaxies are tabulated in Appendix A.

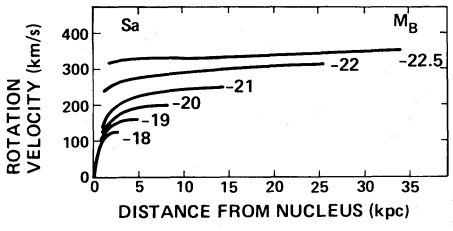

FIG. 5

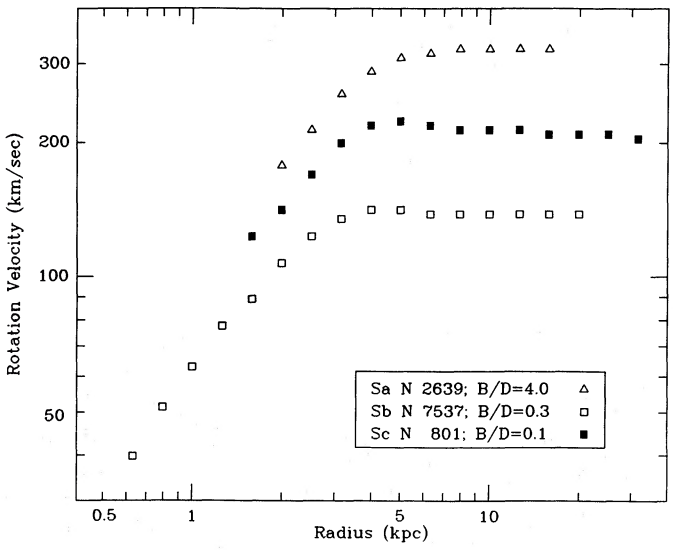

FIG. 6

FIG. 5.—The synthetic Sa rotation curves of Fig. 4 plotted here as a function of linear radius.

FIG. 6.—Rotation curves for an Sa, an Sb, and an Sc galaxy, plotted on a (log V, log R)-scale to emphasize the similarity of form of the rotation curves, even for galaxies of very different morphology. For these three galaxies, the bulge-to-disk ratio ranges from 4.0 to 0.1, yet the shapes of the rotation curves do not reflect these differences.

a) Dependence of Properties on Hubble Type

Within each Hubble type, we have observed galaxies with as large a range of luminosity as we could identify. Hence the sample is not a volume-limited sample but represents the range of galaxy luminosities covered in the RSA (Sandage and Tammann 1981), RC2 (de Vaucouleurs, de Vaucouleurs, and Corwin 1976), and UGC (Nilson 1973), for Sa through Sc galaxies with well-defined Hubble classifications. Somewhat surprisingly, a V/V_m (Schmidt 1968) analysis shows that the majority of the galaxies represent a uniform subset from a magnitude-limited catalog. The distribution of luminosity with Hubble type is shown in Figures 7*a* and 7*b*, for blue and for infrared magnitudes. The distributions of M_B and M_H are very similar, a consequence of the high correlation of B with H (see § IV*c*).

There is little dependence of absolute blue or absolute infrared magnitude on Hubble type in our sample; the range at all Hubble types is 4 mag. This similarity is partly an artifact of our observing requirements, for very low luminosity Sa, Sb, and Sc galaxies are rare in catalogs which are magnitude limited. We were unable to find suitable Sa spiral candidates for study that were fainter than about $M_B = -19$, of suitable apparent magnitude, inclination, and angular size, at the proper observing season.

There is a dependence of V_{max} on Hubble type in our sample (Fig. 7*c*). For Sa's, velocities range from 367 km s^{-1} ($M_B = -22.8$) to 163 ($M_B = -19.3$), compared with 330–144 km s^{-1} for the Sb and 304–99 km s^{-1} for the Sc. The median value of the rotational velocity decreases from 299 to 222 to 175 km s^{-1} from types Sa through Sc. Note, however, the wide overlap

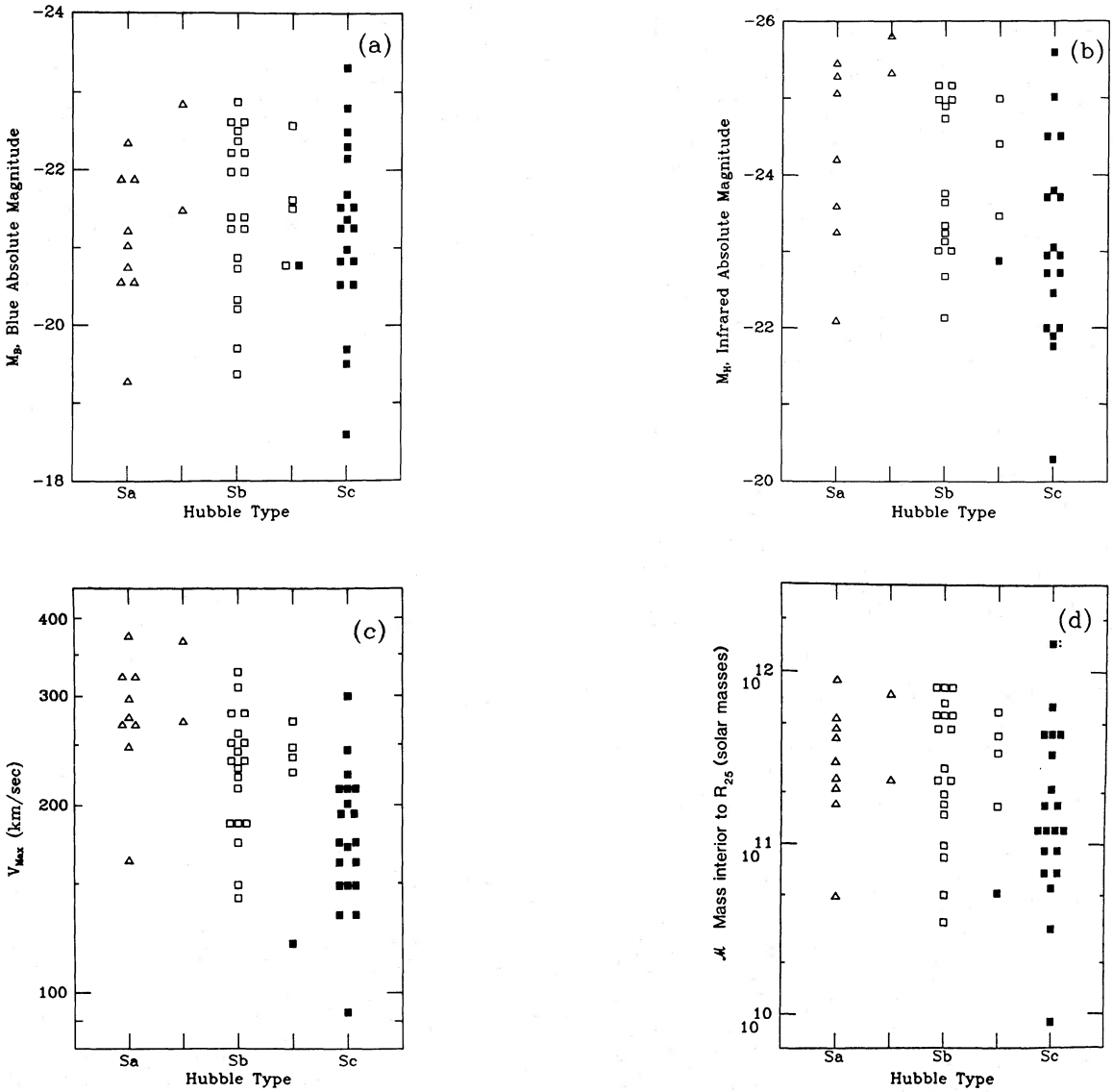

FIG. 7.—(*a*) Distribution of values of blue absolute magnitude M_B as a function of Hubble type for program Sa, Sb, and Sc galaxies. (*b*) Distribution of absolute infrared magnitude, M_H. Note that M_B and M_H distributions are similar to each other, and both distributions are independent of Hubble type. (*c*) Distribution of maximum rotational velocity V_{max} as a function of Hubble type. Note the decrease in values of V_{max} with later Hubble type: median values decrease from 299 to 222 to 175 km s^{-1} from types Sa through Sc. (*d*) Distribution of mass interior to the R_{25} isophotal radius. Although there is a weak Hubble type dependence, an upper limit of about 10^{12} $M_\odot$ exists for all spiral types.

among the Hubble types. The velocity $V_{rot} = 250$ km s^{-1} can identify an Sc of high luminosity, an Sb of intermediate luminosity, and an Sa of low luminosity.

The dependence of the mean value of the mass within the optical image, $\mathcal{M}(R_{25})$, on Hubble type is illustrated in Figure 7*d*. It is interesting and probably significant that the upper limit to the mass of a spiral galaxy is near $10^{12}\ M_{\odot}$, independent of Hubble type.

Estimates of the bulge-to-total luminosity (B/T) for program galaxies have been made by Whitmore (1984). There is a good correlation of B/T with Hubble type, but with considerable overlap among types. Median values of B/T decrease from 30% to 13% to 5% for types Sa, Sb, and Sc, respectively. However, within a single Hubble type, there is no significant correlation of B/T with luminosity or with rotation properties. This is not surprising, in view of the lack of a correlation of Hubble type with luminosity. All correlations which we discuss below are higher as a function of Hubble type than as a function of B/T. With these values of B/T for this sample, an estimate of morphological class is a better indicator of spiral properties than is an estimate of bulge-to-disk luminosity. More quantitative values of B/T are needed to test this conclusion.

b) *Blue Luminosity–Radius Relation*

The relation between blue luminosity and isophotal radius R_{25} for all program galaxies is shown in Figure 8. The Sa galaxies define the same line as the Sb's and Sc's. For our sample, this is the single correlation which shows no separation by Hubble type when blue luminosities are employed. The slope of the relation implies that blue surface brightness is slightly higher for low-luminosity spirals than for high-luminosity spirals. The discrepancy between this slope and that derived by Holmberg (1975) was discussed previously (Paper III). In the infrared, a meaningful independent examination of the luminosity-radius correlation cannot be made, as isophotal galaxy radii at H magnitudes have not yet been measured.

c) *Luminosity-V_{max} (Tully-Fisher) Relation in the Blue and in the Infrared*

The Tully-Fisher (1977, hereafter TF) correlation of luminosity with maximum rotational velocity, V_{max}, is shown in Figure 9*a* for blue luminosities and in Figure 9*b* for infrared luminosities. In the blue, the mean least squares lines have similar slopes of 9.95 ± 1.7, 10.2 ± 2.8, and 11.0 ± 1.8 for the Sa's, Sb's, and Sc's, respectively. (The line is calculated assuming equal errors in each coordinate; the errors are the 1 σ geometrical mean of the errors in the least square lines of X upon Y and Y upon X.) There is, however, a zero-point difference between the Hubble types. At a fixed luminosity, the Sa regression line is displaced $+0.11$ in log V_{max} (a factor of 1.3 in velocity) with respect to the Sb line; the Sc line is displaced about -0.11 in log V_{max} (a factor of 1.3 in velocity). Thus, at a fixed M_B, an Sa has a value of V_{max} which is 1.7 times higher than that for an Sc. At a fixed value of V_{max}, an Sa is about 2 mag fainter than an Sc. For an Sc to exhibit dynamical properties matching those of an Sa, it must be significantly larger and hence brighter than the Sa.

Before evaluating the infrared form of the Tully-Fisher relation, we discuss the H magnitudes for the Sa, Sb, and Sc program galaxies. These magnitudes have been kindly made available by M. Aaronson and are published in Whitmore (1984). The high correlations of the blue and the infrared absolute magnitudes are shown in Figure 10. Least squares mean lines give slopes s near unity and high correlation coefficients r: $s = 1.1 \pm 0.08$ (1 σ of mean), $r = 0.97$ (Sa, $n = 13$);

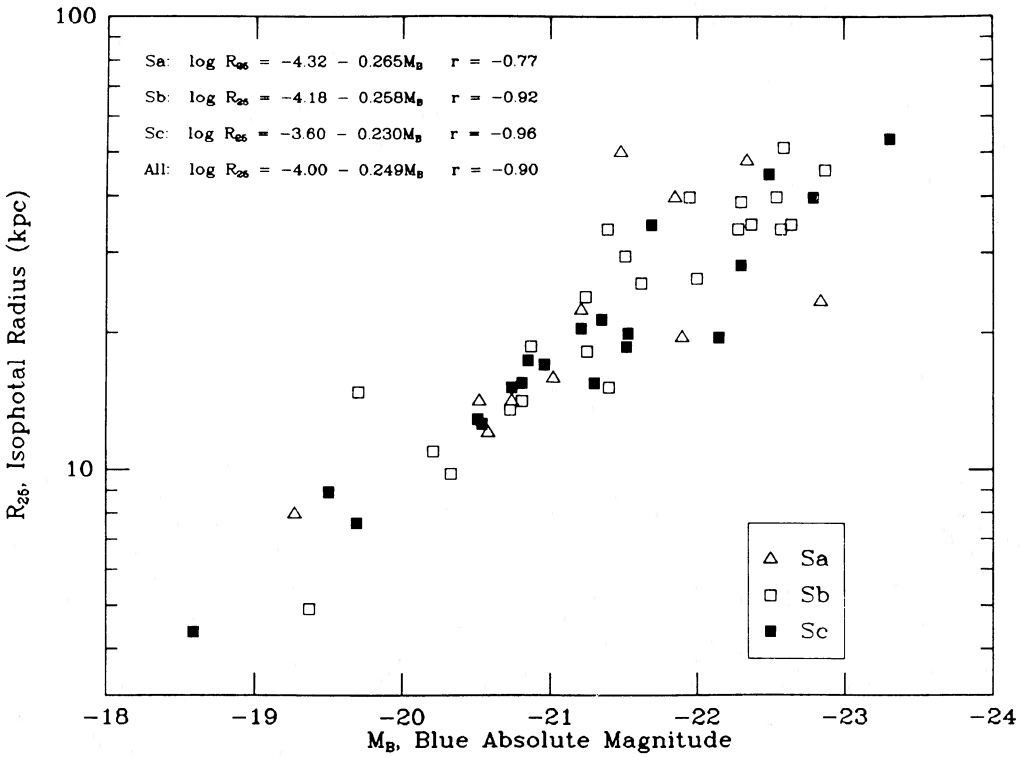

FIG. 8.—Correlation of blue absolute magnitude with linear blue isophotal radius R_{25} for all galaxies in our sample. Note lack of any Hubble type dependence.

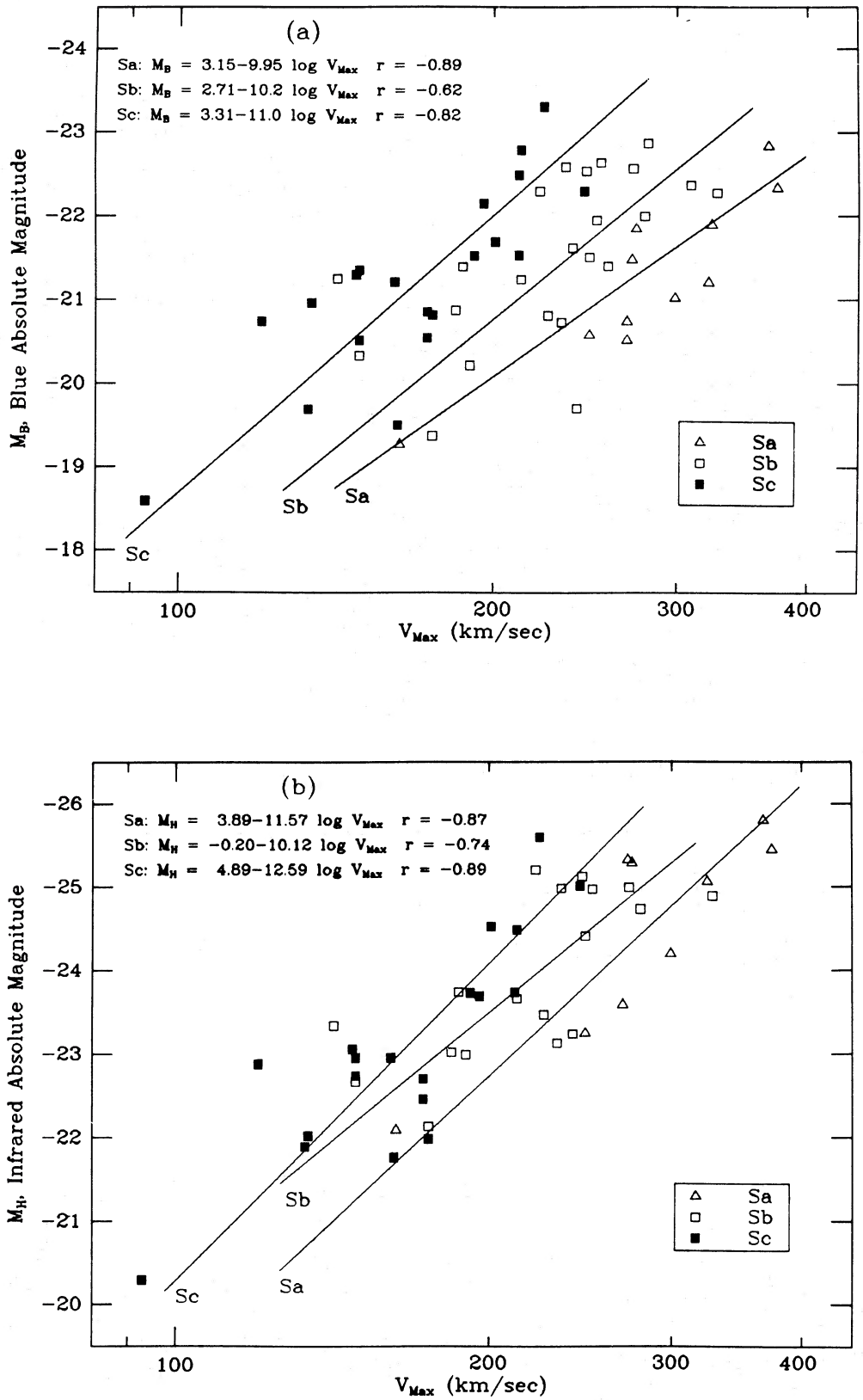

FIG. 9.—The Tully-Fisher relation for our sample. (*a*) Correlation of M_B with V_{max}, the Tully-Fisher relation, for program galaxies. Least squares mean lines for the Sa, Sb, and Sc samples are shown. Each Hubble type independently gives a slope near 10, but with offsets as a function of Hubble type. (*b*) The correlation of M_H with V_{max} for the subset of galaxies in Fig. 9*a* with infrared *H* magnitudes. With infrared magnitudes, also, each Hubble type independently gives a slope near 10, but with offsets as a function of Hubble type. (*c*) The same, but V_{max}-values for Sa's and Sc's have been shifted to eliminate the Hubble type dependence. The 1 σ scatter in M_H is 0.66 mag.

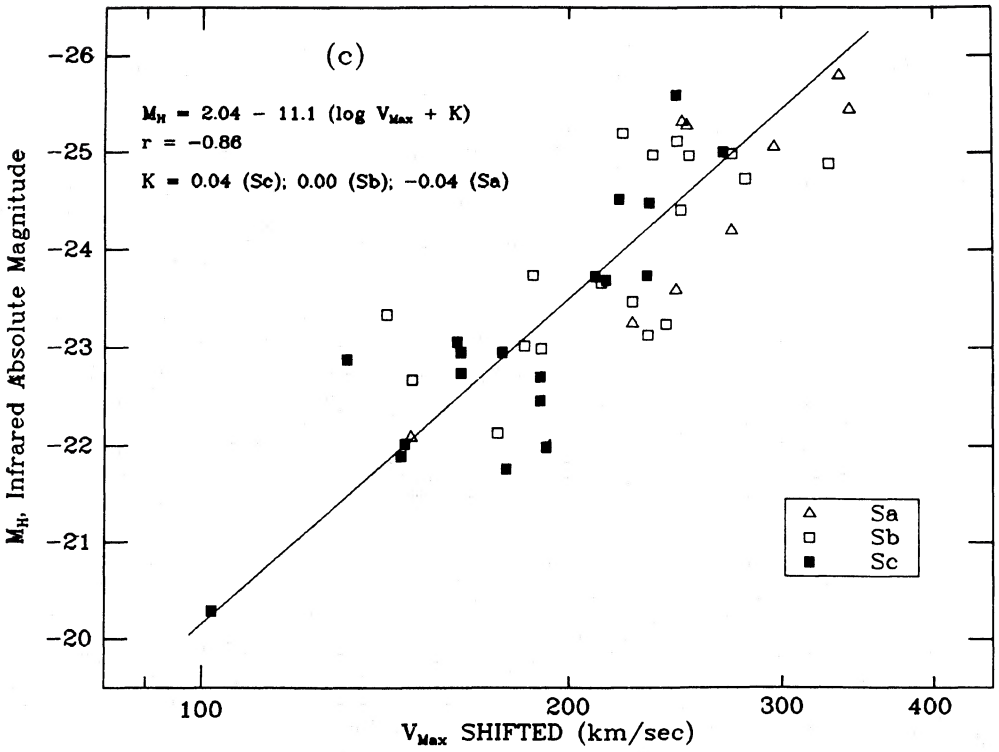

FIG. 9(*c*)

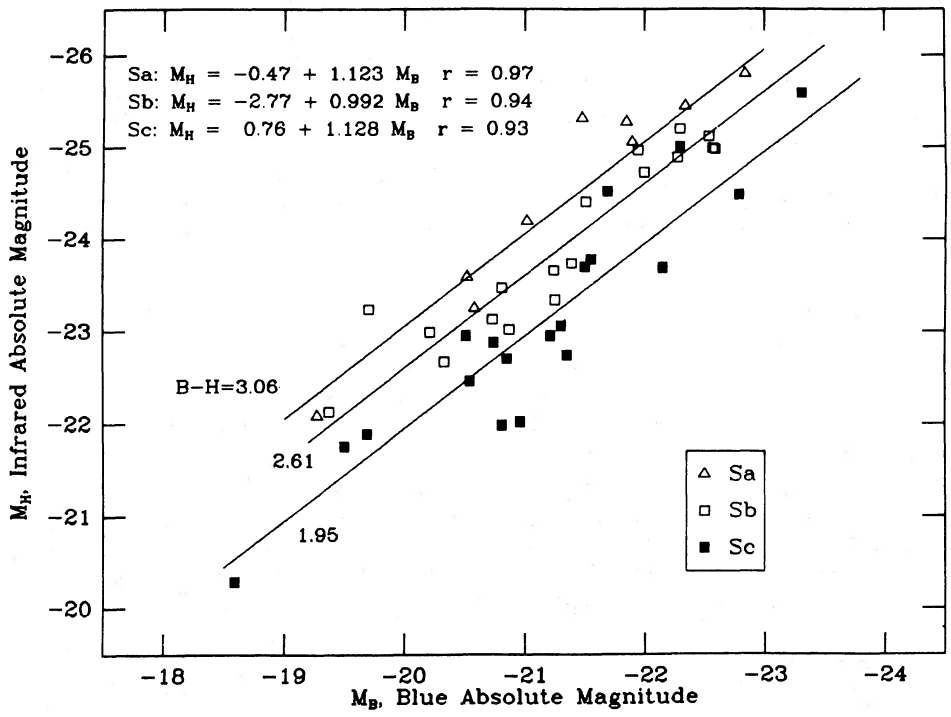

FIG. 10.—The correlation of absolute magnitudes at the H and B bands. Equations for the least squares line fits are listed; coefficients of M_B of unity correspond to a constant $B-H$ value. Best fit lines of constant $B-H$ are drawn for each Hubble type. For program galaxies, there is a good correlation of H with B magnitudes.

$s = 0.99 \pm 0.09$, $r = 0.94$ (Sb, $n = 18$); and $s = 1.1 \pm 0.11$, $r = 0.93$ (Sc, $n = 19$). The proximity of the slopes to unity means that $B^{i,b} - H_{-0.5}$ (which we write $B-H$) is nearly constant for a fixed Hubble type; mean values are $\langle B-H \rangle = 3.06 \pm 0.09$ (1 σ of the mean), 2.61 ± 0.08, and 1.95 ± 0.11 for Sa's, Sb's, and Sc's, respectively. (The use of the hybrid color $B-H$ as a measure of the true color of a spiral galaxy is as valid as using the H magnitude alone for the absolute infrared luminosity.) This correlation of B and H magnitudes indicates that conclusions relating to a single Hubble type are unaltered if H magnitudes are used rather than B, but that relations among various Hubble types will be shifted differentially by the range in $B-H$ with Hubble type. A $B-H$ color offers a good estimate of a spiral Hubble type for this sample.

Because B and H are correlated within a Hubble type, it is no surprise that the zero-point shifts among the Sa, Sb, and Sc galaxies do not disappear from the Tully-Fisher relation with the use of infrared H absolute magnitudes (Fig. 9*b*) although they decrease as expected from the differential decrease of mean $B-H$ with later Hubble type. Using infrared magnitudes, the mean least squares lines have slopes of 11.6 ± 2.5, 10.1 ± 2.3, and 12.6 ± 1.5, similar to each other and similar (at the 1 σ level) to the slopes in the blue. The zero-point difference implies a displacement of $+0.04$ in log V_{max} (a factor of 1.1 in velocity) from Sa to Sb; and of -0.04 in log V_{max} (1.1. in velocity) from Sc to Sb, at a fixed H magnitude.

The mean value of the slope of the Tully-Fisher relation in each passband can be obtained by combining all Hubble types into one relation by removing the zero-point differences among the Hubble types. This is done for the H absolute magnitudes (Fig. 9*c*) by replacing V_{max} with log $V_{max} - 0.04$ (Sa) and log $V_{max} + 0.04$ (Sc). Then the linear least squares fit using all Hubble types has slope of 11.1 ± 1.0, with a correlation coefficient $r = -0.86$. When the Hubble type dependence is removed from the blue absolute magnitude–V_{max} relation [replacing V_{max} with $V_{max} - 0.107$ (Sa) and $V_{max} + 0.111$ (Sc)], the linear least squares fit using all Hubble types has a slope of 10.5 ± 1.3 and a correlation coefficient $r = -0.75$. With either blue or infrared absolute magnitudes, the 1 σ scatter in M is the same: 0.68 mag in M_B and 0.67 mag in M_H.

Thus, for our sample, the Tully-Fisher relation for H magnitudes is essentially identical in slope and in scatter to that for B magnitudes, once the Hubble-type zero-point shift has been removed. The scatter remaining after removing the Hubble type dependence is a measure of the accuracy with which absolute magnitudes may be determined by the Tully-Fisher method. Assuming V_{max} to be error free, then the 1 σ scatter in absolute (B or H) magnitude amounts to 0.7 mag. This is substantially larger than the scatter (~ 0.4 mag) generally observed by Aaronson and colleagues within a *single* cluster of galaxies. In part, the smaller scatter arises by placing all galaxies at the mean cluster distance, and thus eliminating random distance errors. The larger scatter found here for field galaxies may indicate a larger cosmic scatter in the properties of field galaxies compared with cluster galaxies, or it may indicate the uncertainties in estimating distances to field galaxies based on a smooth Hubble flow. We defer until § V a more complete discussion of the differences between the optical and 21 cm galaxy samples.

d) The Luminosity-Mass Correlation

The correlation of mass contained within the optical isophotal radius, $\mathcal{M}(R_{25})$, with absolute blue luminosity (Fig. 11*a*) extends our earlier result for Sb and Sc galaxies. The mass–to–blue luminosity $\mathcal{M}/L_B$ ratio is virtually constant for a given Hubble type and is higher for the earlier Hubble types. Least squares linear fits to each Hubble type produce high correlations and slopes near unity (Fig. 11*a*). Logarithmic mean values of $\mathcal{M}/L_B$ of 6.2 ± 0.6 (1 σ of mean) for Sa's, 4.5 ± 0.4 for Sb's, and 2.6 ± 0.2 for Sc's are good approximations to the least squares fits. Thus $\mathcal{M}/L_B$ contains Hubble type information but essentially no luminosity information.

This result is a necessary consequence of the lack of a Hubble type dependence between $R_{25}^{i,b}$ and luminosity and the dependence of the mean value of V_{max} on Hubble type. Since mass $\mathcal{M}$ is proportional to $V_{max}^2 R$, $\mathcal{M}/L$ is proportional to $V_{max}^2(R/L)$; it follows that $\mathcal{M}/L_B$ at each Hubble type is proportional to V_{max}^2. Thus, $\mathcal{M}/L_B$ is predicted to be $1.28^2 = 1.6$ larger for an Sa than for an Sb, and $1.29^2 = 1.7$ times larger for an Sb than for an Sc (§ IV*c*). The observed values (Fig. 11*a*), $6.2/4.5 = 1.4$ and $4.5/2.6 = 1.7$, are close to these predicted values.

The definition of mass-to-light ratio must be altered when infrared H magnitudes are used instead of blue magnitudes. The H magnitudes used in this paper are measured at a radius of $\frac{1}{3}R_{25}$ (Aaronson, Huchra, and Mould 1979) and therefore do not measure the luminosity over the entire region for which we measure the mass (i.e., interior to R_{25}). On the other hand, the combination of H magnitudes and masses will yield reliable *relative* values of $\mathcal{M}/L_H$. For our calculations, we take the absolute solar H magnitude to be 3.68.

The correlation of mass with H infrared luminosity (Fig. 11*b*) exhibits little Hubble type dependence, in contrast to the correlation of $\mathcal{M}/L_B$ with Hubble type. Logarithmic means of $\mathcal{M}/L_H$ are 2.3 ± 0.2 (1 σ of mean), 2.2 ± 0.2, and 1.7 ± 0.3 for Sc, Sb, and Sa types, respectively. A least squares fit of $\mathcal{M}(R_{25})$ upon M_H for galaxies of all Hubble types combined has a slope of 0.84 ± 0.05 and a correlation coefficient of $r = -0.94$. The slope smaller than 1 implies that mass increases slightly more slowly than IR luminosity. However, the derived slope is within 3 σ of unity, so that adopting $\mathcal{M}/L_H$ as constant is a fair approximation for our sample, independent of luminosity and Hubble type. This lack of dependence of $\mathcal{M}/L_H$ on Hubble type is not inconsistent with the dependence of $\mathcal{M}/L_B$ on Hubble type. It does require, however, that the correlation of infrared H luminosity and radius have a Hubble type dependence, contrary to the lack of Hubble type dependence which is observed in the blue.

We show in Figure 11*b* a line of $\mathcal{M}/L_H = 2.1 \pm 0.1$, the best fit to all the data. It is surprising, but useful, that the H luminosity is such a good measure of the mass interior to R_{25}, independent of spiral type. An Sa and an Sc of equal H luminosity will have equal masses interior to R_{25}, but R_{25} is smaller and V_{max} is higher for the Sa. As we have concluded previously, the Hubble sequence, as evidenced from our sample, is a sequence of decreasing density from type Sa to type Sc.

For an Sa and an Sc of equal blue luminosity, the Sa will contain a more extensive red stellar population, a higher H luminosity, a mass larger by the amount of the ratio of their $\mathcal{M}/L_B$ values (6.2/2.6), and a higher V_{max}.

e) What Fraction of the Mass Is Not in the Disk?

The rotation curves we have obtained for Sa, Sb, and Sc galaxies bear little relationship to the rotation curves which would be predicted from the distributions of optical luminosity in these galaxies. This surprising observation leads us to ask

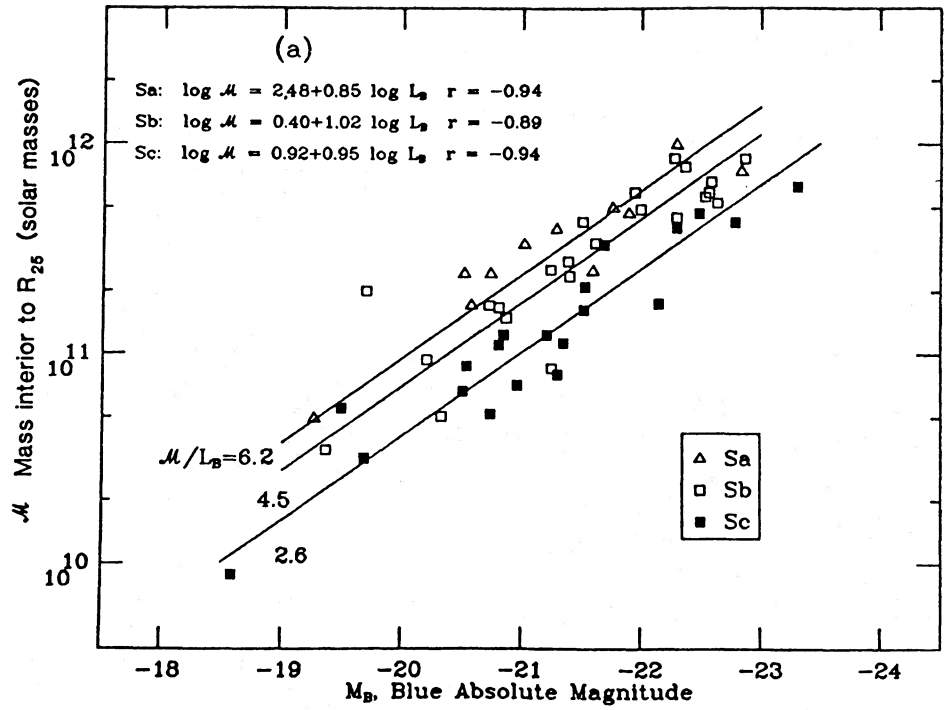

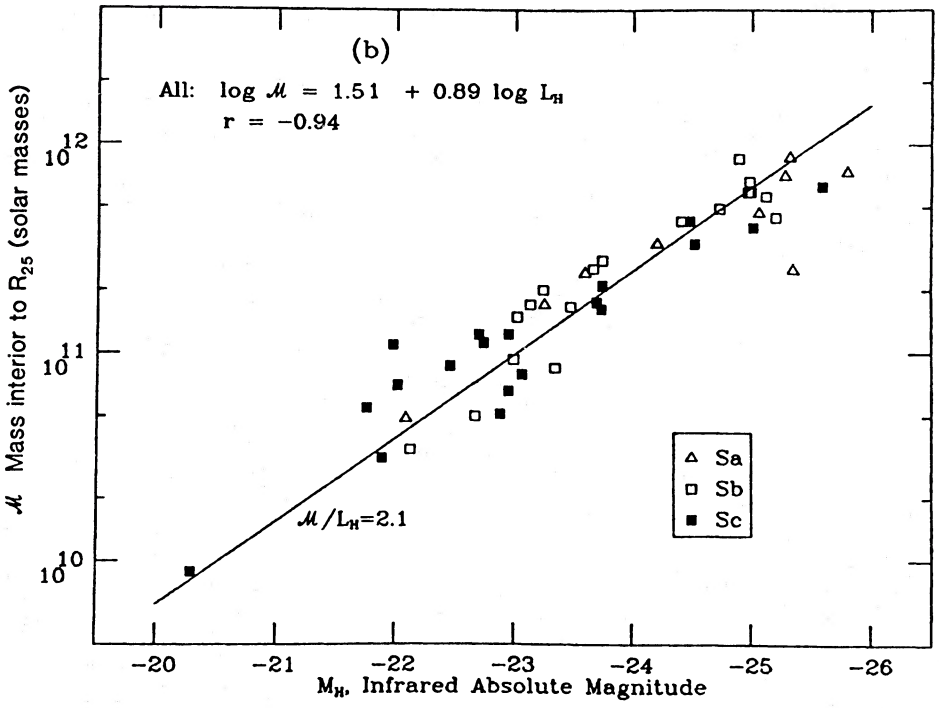

FIG. 11.—Correlation of mass with luminosity for program galaxies. (*a*) The correlation of $\mathcal{M}(R_{25})$ with M_B. Equations for least squares line fits are listed; coefficients of log L_B of unity correspond to constant $\mathcal{M}/L$. Best fit lines of constant $\mathcal{M}/L_B$ are shown for Sa, Sb, and Sc samples. (*b*) The correlation of $\mathcal{M}(R_{25})$ with M_H. The use of the hybrid H magnitude removes most of the Hubble type dependence in the mass-to-H luminosity ratio. The best fit line of constant $\mathcal{M}/L$, $\mathcal{M}(R_{25})/L_H = 2.1$, is shown.

what fraction of the mass of a spiral galaxy *is* contributed by material not in a disk.

We first discuss this question in relation to our Galaxy. The recent analysis of number densities of F and K stars above the galactic disk in the solar vicinity (Bahcall 1984*a*, *b*) indicates that $(\mathcal{M}/L_V) \sim 3 \pm 1$ in the galactic disk; only half of this mass is "counted" in stars, H I, H II, and dust. Because the color of an Sbc disk is approximately the same as that for the Sun, $B-V = 0.65$, $L_B \sim L_V$ for the galactic disk. Bahcall's result, combined with the values above, which give $\mathcal{M}/L_B$(dynamical) = 4.0 for an Sbc, implies that only a small fraction, perhaps 25%, of the mass is not in the disk. However, it is premature to draw any firm conclusions from these values, for this fraction is imprecise (and likely a lower limit) for several reasons, in addition to the uncertainty in the Bahcall number. The high rotational velocity for our Galaxy, $V_{max} > 250$ km s^{-1}, suggests that the Galaxy is closer to type Sb than Sc. A velocity of 250 km s^{-1} is a *very* high rotational velocity for an Sc and even for an Sbc galaxy. Second, our calculated values of $\mathcal{M}/L$ scale with the Hubble constant H_0, while those derived by Bahcall are H_0 independent. Thus, for $H_0 = 75$ km s^{-1} Mpc^{-1}, $\mathcal{M}/L_B$(dynamical) = 6 (Sbc) and = 7 (Sb). Using these values, the percent of halo mass within R_{25} is near 50%. Although this comparison of the inferred value of $\mathcal{M}/L$ in the solar vicinity and the calculated $\mathcal{M}/L$ for various Hubble types does not put a very tight constraint on the fraction of matter in the halo of a typical spiral, it does suggest that the fraction is not dominant, interior to R_{25}.

A second constraint on the mass distribution comes from combining the blue mass-to-light ratios calculated in § IV*d* with estimates of mass-to-light ratios from model stellar populations (e.g., Larson and Tinsley 1978). Mean $B-V$ colors are 0.75 (Sa), 0.64 (Sb), and 0.52 (Sc; de Vaucouleurs 1977). For these $B-V$ colors, the Larson-Tinsley models yield ratios of $\mathcal{M}_{lum}/L_B$ of 3.1:2.0:1.0 for Sa:Sb:Sc types.

The *observed* ratio of $\mathcal{M}/L_B$ of *all* (dynamical) mass within R_{25} is 2.4:1.7:1.0 for Sa:Sb:Sc types. If allowance is made for the fact that Sc's contain, on average, more gas than do Sa's (e.g., Roberts 1975), then the ratio of $\mathcal{M}/L_B$ observed here to $\mathcal{M}_{lum}/L_B$ predicted from stellar models is approximately independent of Hubble type. The values of $\mathcal{M}/L$ found here suggest that the ratio of dark-to-luminous matter derived for our Galaxy applies equally well to other spirals, independent of morphological type.

An estimate for the *absolute* value of $\mathcal{M}_{lum}/L_B$ comes from Larson and Tinsley's population models. Their calculations indicate that the average $B-V$ colors for Sc galaxies correspond to a $\mathcal{M}_{lum}/L_B = 1.0$. This value is likely to be an underestimate, due to effects of internal extinction by dust, and to underestimating the luminosities contributed by the low-mass end of the stellar mass function. But the approximately constant ratios of $\mathcal{M}/L_B$ values determined dynamically [6:4:2] with $\mathcal{M}_{lum}/L_B$ values predicted from stellar models [3:2:1] suggest that $\mathcal{M}/\mathcal{M}_{lum}$ is of order 2, independent of Hubble type and luminosity.

One additional piece of evidence that interior to R_{25} the halo mass and the disk mass are of the same order of magnitude comes from the detailed study of the mass distribution within NGC 3198, an Sc galaxy for which the 21 cm rotation curve extends to $2.7R_{25}$ (van Albada *et al.* 1984). These authors show that to place more than 56% of the total mass in the disk interior to R_{25} would require an implausible halo with a hollow core. Their models do permit, however, a *smaller* mass fraction to reside in the disk.

All of these considerations suggest that the visible material in spiral galaxies contributes of order half of all the mass within the optically defined isophotal radius. It is likely that the dark matter consists of at least two components: one disklike, the other arranged in a more nearly spherical distribution. Since the disk mass is much more centrally concentrated than the total mass, the disk mass must be *the* dominant mass component over a significant portion of the visible galaxy. Why then do we not see the transition from disk to nondisk mass distributions within a spiral galaxy reflected more prominantly in the rotation curve? The answer to this question may be central to our understanding of the structure of spiral galaxies, yet it has taken many years of effort just to be able to pose the question. More detailed study of mass components and overall mass forms (Burstein and Rubin 1985) should elucidate the answers.

V. PROPERTIES OF GALAXY SAMPLES OF RUBIN *et al.* AND AARONSON *et al.*

The properties which we have deduced for our sample of 54 spiral galaxies differ markedly from those deduced by Aaronson and his colleagues for a sample of 308 spiral galaxies (e.g., Aaronson *et al.* 1982; Aaronson and Mould 1983). However, the composition of the two samples differs in three very major respects: (1) Classifications for the galaxies in the Aaronson *et al.* sample (hereafter A^+) come from the RC2, with a few from the UGC. Only 15 A^+ galaxies are classified Sa or Sab. Of these, only eight are classified Sa or Sab in the RSA; three are classified Sb; six are classified Sb in the UGC. Thus these Sa's clearly do not have impressive Sa-type morphologies. It is not surprising then that the highest rotational velocity for an Sa/ab galaxy in the A^+ sample is 269 km s^{-1} (for M81, elsewhere classified Sb). In contrast, 9 of the 11 Sa galaxies in our sample have rotational velocities ranging from 269 to 374 km s^{-1}, i.e., higher than any Sa or Sab in the A^+ sample. (2) The A^+ sample contains significant numbers of Scd, Sd, and Irr galaxies, all of low luminosity. None of these types are included in our sample. (3) The A^+ sample is an H I–rich sample, consistent with their criterion that the 21 cm profile have a high signal-to-noise ratio.

Ignoring these differences for the moment, we find the following:

1. For our sample, although the mean value of V_{max} increases with earlier Hubble type, the mean absolute magnitude (B or H) is independent of Hubble type. For the A^+ sample, both mean V_{max} and mean H luminosity are higher for earlier Hubble types.

2. For our sample, the slope of the Tully-Fisher relation is the same for B and H magnitudes, and is independent of Hubble type and color. Of major importance, the zero point of the Tully-Fisher relation is a function of Hubble type in both passbands. For the A^+ sample, the slope in the Tully-Fisher relation is smaller using B than using H magnitudes, and no significant zero-point difference is evident as a function of Hubble type in either passband.

3. For our sample, the mass–to–*blue* luminosity ratio interior to R_{25} is approximately constant within a Hubble type but varies systematically with type, increasing from 2.6 ± 0.2 for Sc's to 6.2 ± 0.6 for Sa's. The mass–to–*infrared* H luminosity ratio is virtually the same for all galaxies, independent of Hubble type, and equal to 2.1 ± 0.1. In contrast, the galaxies in the A^+ sample have a correlation of $\mathcal{M}/L_H$ with both Hubble type and V_{max} (e.g., Burstein 1982).

4. For our sample, $B-H$ color is strongly correlated with Hubble type, becoming bluer with later Hubble type, but is only weakly correlated with B or H absolute magnitude. Our data do not support the conclusion of Tully, Mould, and Aaronson (1982) that $B-H$ is solely a luminosity indicator, independent of Hubble type. In fact, in the A^+ sample, $B-H$ is correlated both with H luminosity and with Hubble type. These differences in color-luminosity relations are a direct consequence of the differences in the Hubble type and Tully-Fisher relations in these samples. We now discuss this last point in more detail.

For our galaxies, $B-H$ is a better diagnostic of Hubble type than of luminosity. There is *some* luminosity information in $B-H$, as the slopes greater than unity ($s = 1.12$, 0.99, and 1.13 for Sa, Sb, and Sc, respectively) show: especially for the Sa's and Sc's, slightly higher values of $B-H$ accompany higher luminosities. Statistical tests (Spearman rank correlations, least squares correlations) indicate that Hubble type has about twice the weight of H luminosity in determining $B-H$. For our sample, it is difficult to predict a galaxy's luminosity for almost any $B-H$ value; we could do better in predicting its Hubble type.

Using a principal component analysis, Whitmore (1984) has shown that the differences between our sample and the A^+ sample are decreased by about 50% if the A^+ sample is restricted to types Sa, Sb, and Sc (but note that it is then primarily an Sb, Sc sample). Appeal to distance errors or sparseness of data cannot explain the remaining differences. We believe that the source of the remaining differences must lie in the manner in which the samples were selected.

The principal difference in the selection processes for these two samples comes from the use of the H I velocity profiles as a criterion for selection by Aaronson *et al.* A galaxy must have a high signal-to-noise 21 cm profile to be included in their sample. Clearly, such a discriminant involves the rotation velocity itself: for equivalent H I fluxes, the galaxy with smaller V_{max}, and hence narrower profile, will be more easily detected than the galaxy with higher V_{max}. It is probable that the use of the H I profile signal-to-noise ratio as a selection criterion narrows the sample of galaxies to a restricted region in parameter space in which the H I content of galaxies correlates in a limited way with Hubble type, with rotation velocity, and with absolute magnitude.

The biases for the Rubin *et al.* sample (Papers I, II, and here) are very different. Galaxies were chosen to be nonbarred, to be easily classifiable, and to be generally isolated or at most in small loose groups. Because we wished the largest range in luminosity with Hubble type, we had to sample galaxies over a large volume of space and environments.

In an effort to examine the biases and the space distribution of the galaxies in our sample, we have performed a V/V_m analysis (Schmidt 1968; hereafter we write Vol/Vol$_m$ to prevent confusion of notation with velocity) and have compared the results with a similar analysis of the RC2 (Meisels and Ostriker 1984).

Results indicate that the galaxies in the Rubin *et al.* sample represent a fair subset of a magnitude-limited sample. Specifically, values of $\langle \mathrm{Vol/Vol}_m \rangle$ (which are 0.5 for a complete sample) are 0.5 for Sa, Sb, and Sc types separately, and for galaxies of high luminosity and of low luminosity separately, regardless of Hubble type (Table 3). Apparently faint program galaxies have the same distribution in absolute magnitude as do the apparently bright ones. The whole sample has the desirable trait that there is no correlation of M_B and Vol/Vol$_m$. Solutions for the Tully-Fisher correlation using the complete subset to $m = 12.6$ have slightly steeper slopes than those found for the entire sample, but the differences are probably not significant because of the small sample size. In contrast, the RC2 is a less complete magnitude-limited sample, and the A^+ sample especially so. The present analysis emphasizes quantitatively what has already been stated above. The differences in the Rubin *et al.* and the Aaronson *et al.* results arise from the very different samples. To a fair approximation, the Rubin *et al.* sample is a subset of a magnitude-limited catalog; the A^+ sample is not, nor was it ever intended to be.

However, the positive results from this analysis do not lessen our concern that some other galaxy property, such as high blue surface brightness, may have caused us to choose an unrepresentative sample of galaxies. A challenge for the future will be to see how truly global are the correlations deduced from each of these samples.

VI. CONCLUSIONS

For 54 Sa, Sb, and Sc galaxies, we have determined rotational velocities over most of the optical extent of the galaxies. The sample covers the largest range of luminosity within each Hubble type that we could identify, and thus is not characteristic of a fixed volume of space. From this material, we draw the following conclusions.

1. Sa rotation curves exhibit a similar progression with

TABLE 3

AVERAGE VALUES OF VOL/VOL$_m$ FOR Sa, Sb, AND Sc GALAXIES

SAMPLE	$\langle \mathrm{Vol/Vol}_m \rangle$ Sa	Sb	Sc	All	B_T LIMIT	% OF SAMPLE
Rubin *et al.*[a]	0.50 ± 0.11(11)	0.52 ± 0.06(13)	0.47 ± 0.09(11)	0.50	12.6	58
RC2	0.41 ± 0.02(232)[b]		0.43 ± 0.02(203)[b]	0.42[b]	12.5[b]	76[b]
Aaronson *et al.*[c]	0.12 ± 0.03(11)	0.34 ± 0.04(66)	0.41 ± 0.04(70)	0.36	12.6	60
Rubin *et al.*[a]	apparently bright ($B_T \leq 12.6$) $\langle M_B \rangle = -21.3 \pm 0.2$ absolutely bright ($M_B \leq -21.2$) $\langle \mathrm{Vol/Vol}_m \rangle = 0.48 \pm 0.06$		apparently faint ($B_T > 12.6$) $\langle M_B \rangle = -21.5 \pm 0.2$ absolutely faint ($M_B > -21.2$) $\langle \mathrm{Vol/Vol}_m \rangle = 0.51 \pm 0.08$			

[a] Papers I, II, and here.
[b] Meisels and Ostriker 1984.
[c] Aaronson *et al.* 1982.

luminosity as do the Sb and Sc galaxies. Sa galaxies of low luminosity generally have low central velocity gradients and low rotational velocities, V_{max}, in contrast to Sa galaxies of high luminosity, which have high central velocity gradients and high values of V_{max}.

2. The forms of the rotation curves exhibited by the Sa's are markedly similar to those found previously for the Sb and Sc galaxies. Mean, synthetic rotation curves vary systematically with luminosity within a Hubble type, but the forms are generally similar for the Sa's, Sb's, and Sc's.

3. The overall similarity of forms of the rotation curves for spirals of very different morphologies, coupled with the derived values for the dynamical mass-to-luminosity ratios, implies that both the dark halo mass and the disk mass contribute to the total mass distribution at all radii within the optical galaxy. Among spirals of very different morphologies, the form of the mass distributions must differ only by scaling factors.

4. While the approximately 4 mag range is similar within each Hubble type, the values of V_{max} increase with earlier Hubble type. Median values of V_{max} increase from 175 km s^{-1} (Sc) to 299 km s^{-1} (Sa). At every radius, an Sa has a higher mass density than an Sb or Sc of equivalent luminosity.

5. Absolute blue magnitude M_B and absolute infrared magnitude M_H are correlated for all Hubble types. Mean values of $B-H$ are 3.1 ± 0.1 (Sa), 2.6 ± 0.1 (Sb), and 1.9 ± 0.1 (Sc). $B-H$ is a good estimator of Hubble type and a poorer estimator of luminosity.

6. The luminosity–log V_{max} (Tully-Fisher) correlation has a slope 10 ± 2 for each Hubble type, but with zero points displaced for each type. At equal blue luminosity, V_{max}(Sa) is 1.7 times higher than V_{max}(Sc). At equal values of V_{max}, an Sa is about 2 mag fainter in the blue than an Sc. The offsets are decreased, but not eliminated, when infrared H luminosities are used. At equal H magnitudes, V_{max}(Sa) is 1.3 times higher than V_{max}(Sc). At equal V_{max} an Sa is over 1 mag fainter in H than an Sc. Slopes for the infrared Tully-Fisher relation are 11 ± 2 for each Hubble type.

7. The ratio of mass, interior to R_{25}, to blue luminosity is nearly constant within a Hubble type, independent of luminosity: $\langle \mathcal{M}/L_B \rangle = 6.2 \pm 0.6$ (Sa), 4.5 ± 0.4 (Sb), and 2.6 ± 0.2 (Sc). In contrast, $\langle \mathcal{M}/L_H \rangle$ is almost independent of both luminosity *and* Hubble type. A value of $\langle \mathcal{M}/L_H \rangle = 2.1 \pm 0.1$ is a surprisingly good measure of mass interior to R_{25}.

8. A comparison of values of $\mathcal{M}/L$ derived here with those predicted from model stellar populations offers weak evidence that the ratio of dark-to-luminous matter is not a function of Hubble class, and that $\mathcal{M}/\mathcal{M}_{lum} \sim 2$ interior to R_{25}.

9. The correlations among the physical properties of the galaxies in our sample are demonstrably different from those in the H I–selected samples, such as those of Aaronson *et al.* These differences persist when infrared magnitudes are used in place of blue magnitudes and are probably the product of selection effects in the choice of galaxy samples. For the Rubin sample of galaxies, a V/V_m analysis shows that a majority of the galaxies represent a uniform density distribution selected from a complete catalog which is magnitude limited at 12.6; the apparently fainter galaxies are distributed over all absolute magnitudes.

We thank the directors of Cerro Tololo Inter-American Observatory, Kitt Peak National Observatory, Las Campanas Observatory, and Lowell Observatory for telescope time. We have benefited from conversations with many colleagues while this work was in progress, and thank especially Dr. David Koo for valuable comments on the manuscript, and Drs. A. Sandage and F. Schweizer for use of their photographs. V. C. R. thanks Dr. John Bahcall and the Institute for Advanced Study for their hospitality, which contributed to the completion of this paper. D. B. acknowledges support from an Arizona State University Faculty Grant-in-Aid.

APPENDIX A

Table 4 contains the adopted rotation velocities for the Sa, Sb, and Sc galaxies in our samples. The listed velocity is the mean of all measures within each radial bin; the listed error is 1 σ of the mean. Velocities for the Sa galaxies are presented here for the first time. In Figure 12 we show the measured velocities for the two sides of the major axis superposed in order to illustrate the degree of symmetry within each Sa galaxy. This statistical procedure has introduced some differences in the velocities tabulated here from velocities read from hand-drawn curves (Papers II and III).

For the Sb galaxies, we correct the following typesetting errors in Table 4, Paper II. For galaxies N7537, U11810, N7171, and N7217 (lines 8–11), all entries for $R > 16$ kpc belong to the galaxy one line above on the table. For N1417 (line 16), velocities for $R = 22$ and 26 kpc were omitted. All calculations were made with the correct velocities, which are shown here. Data for Sc galaxies come from our previous lists in Papers I and III; velocities for UGC 2885 include the correction noted in Paper II.

All other data remain as published, except for small changes in the adopted extinction (Burstein and Heiles 1984) or inclination for a few galaxies. All changes are detailed in Table 5.

NOTE TO TABLE 4.—Velocities in km s^{-1} are formed from mean of all measured velocities within the radial bin, projected to the plane of the galaxy and corrected for the relativistic Doppler shift, $1/(1 + z_0)$. Mean radial distance for first bin is indicated in parentheses following velocity. Listed error is 1 σ of the mean.

TABLE 4

ROTATIONAL VELOCITIES FOR Sa, Sb, AND S

		0.5	1.0	1.5	2.1	3	4	5	6	7	8.2	10	12
													<Radiu
Sa													
NGC 1024	11±4(0.02)	117	204	171±48	205±31	236	...	...	...	...	260±7	261±4	254±4
NGC 1357	...	...	170±20	209±24	244±8	212±13	219±13	235±4	265±5	267±13	252±12	259±5	
NGC 2639	...	...	...	...	179±3	249±7	286±4	309±4	318±4	318±3	323±2	319±4	318±4
NGC 2775	...	...	...	...	253	269±5	272±6	289±2	303±4	284±2	291±5	270±4	
NGC 2844	6(0.01)	85±4	113±4	137±2	153±5	160±4	141±4	153±3	148±10	171			
NGC 3281	...	...	...	...	182	199±5	191±8	186±3	187±12	184	209±12	203±10	226
NGC 3593	27±5(0.11)	85±3	108±4	110±4	101±4								
NGC 3898	...	166	147±30	205	198	207±4	211±1	219	240±5	240±5	249±4	259±3	244±5
NGC 4378	...	207±26	281±9	314±21	327±21	317±19	316±10	319±10	309	...	...	308±1	329±4
NGC 4419	-3±7(0)	88±6	124±8	150±9	169±2	177±3	187±3						
NGC 4594	201±16(0.38)	47±16(0.74)	94±12	105±13	176±7	259±7	334±9	322±8	331±6	340±9	304±3	324±6	359±9
NGC 4698	...	57	120±6	112±22	156±7	172±4	192±3	190±2	215±3	234±4	252±5		
NGC 4845	46±11(0.11)	136±8	184±4	203±3	201±6	161±7	170±11	181±4	181±7	181±1			
NGC 6314	...	...	...	231±2	...	232±6	248±6	245±4	...	...	216±4	233	225±5
IC 724	...	...	...	...	...	376	347	369±9	346	343	328	...	...
UGC 10205	-24±2(0.10)	...	59	83±29	98	160±17	...	201±6	194	215±9	218±5	217±2	238±2
UGC 10205						-20	-23±9	-16±16	2	7±11	92±3	164±7	
UGC 10205								130	52				
Sb													
NGC 1085	...	...	...	253±13	270±8	292	295±5	306±3	302±5	304±3	303±8	292±3	297±3
NGC 1325	-15±5(0.06)	54±5	82±7	93±4	107±3	121±3	131±2	134±2	149±1	158±4	163±2	165±2	179±2
NGC 1353	11±3(0.04)	140±5	154±4	...	207	...	174	189±3	191±6	234	229±9		
NGC 1417	34±84(0.01)	...	188±38	225±17	248±11	256±4	260±4	266±2	269±2	264±5	281±2	261±5	270±5
NGC 1515	35±10(0.05)	115±9	196±10	229	...	...	204±1	163±7	172±3	162±3	164±2	149±3	165±3
NGC 1620	...	77±16	113	94±18	135±4	158±2	180±2	177±3	173±6	181±3	202±3	212±3	212±1
NGC 2590	broad	broad	broad	broad	broad	...	221±27	211±13	207±3	201±2	203±5	220±3	234±4
NGC 2708	broad	93±5	95±8	103	120±7	...	214	162±3	193±14	225±2	239±4	227±4	
NGC 2815	13±15(0.0)	280	232±21	271	269±3	279±8	297	296	267±7	274±4	271±3	266±2	...
NGC 3054	...	...	48	82	74±14	132±10	173±25	172	183±11	199±8	...	220±4	238±6
NGC 3067	17±8(0.13)	56±4	87±2	104±2	119±1	127±1	129±1	138±2	142±1	148±1			
NGC 3145	...	226±2	203±1	...	...	...	...	238±2	218±11	240	251±5	266±4	255±4
NGC 3200	44(0.10)	103±64	161±22	219	280	263±1	237±12	221±17	217±10	245±8	253±3	263±5	268±5
NGC 3223	...	...	45±10	75	...	...	228±6	236±8	243±5	253±4	239±8	236±5	246±7
NGC 4448	3±1(0.01)	...	...	...	163±7	179±2	183±2	190±4	197±1	187±3			
NGC 4800	32±40(0.12)	134±4	146±2	148±2	165±2	173±2	169±5						
NGC 7083	...	...	...	...	165±15	194±7	194±3	180±18	203±9	191±8	215±5	214±5	214±9
NGC 7171	26±9(0.01)	12±11	9	...	65	107	173±13	189±9	187±23	213±18	212±1	211±7	216±7
NGC 7217	...	...	212±7	254±5	284±5	266±7	268±3	...	265±3	284±4	267±6	241±4	
NGC 7537	4±4(0.10)	30±3	66±8	84±5	108±2	134±2	142±3	139±5	140±4	139±2	138±1	132±1	143±2
NGC 7606	-4(0.0)	...	...	...	...	...	189	211±4	225±5	243±3	257±3	270±3	273±1
UGC 11810	1±3(0.0)	...	84±2	104	128±1	116	131±4	146±6	...	161±5	164±4	164±5	173±4
UGC 12810	25±79(0.05)	56±38	...	...	...	...	...	...	...	...	...	183	208±3
Sc													
NGC 701	53±3(0.07)	61±2	51±2	62±1	85±2	89±3	108±3	125±3	141±4	151±3	139		
NGC 753	...	142±5	180	...	153±12	168±3	176±7	195	210±9	209±11	203±4	201±5	204±1
NGC 801	...	...	...	119±1	137±16	198±2	221±8	230±2	...	211	205±3	212±5	227±8
NGC 1035	10±1(0.15)	34±2	65±3	80±3	90±3	106±3	121±1	122±2	125±3	133±3			
NGC 1087	-6±8(0.08)	49±17	88±6	98±4	112±3	119±4	118±4	115±3	109±4	118±6	132±2	136±3	
NGC 1421	37±16(0.19)	78±6	100±4	122±7	160±7	175±2	168±4	160±8	145±9	150±8	155±6	158±4	162±4
NGC 2608	1±1(0.01)	108±9	122	...	109±1	...	97	...	109±6	110	100±6	...	132
NGC 2715	32±13(0.09)	53±3	72±5	88±8	94±3	106±2	116±1	124±2	134±1	139±1	153	140±2	137±2
NGC 2742	15±7(0.08)	67±5	93±9	107±5	114±5	130±2	136±2	151±3	159±2	159±4	165±2	173±4	
NGC 2998	...	86±10	...	120±4	...	142±2	167±7	193±5	196±2	199±2	182±5	188±2	197±4
NGC 3495	7±8(0.168)	43±4	57±3	66±2	77±2	90±4	118±2	128±3	135±4	129±3	149±5	167±3	171±4
NGC 3672	1±2(0.03)	8±6	28±4	...	60±6	120±10	162±17	175±10	166±3	182±4	182±3	185±7	172±3
NGC 4062	39±6(0.08)	73±6	94±4	105±2	121±3	129±2	142±3	148±2	162±3	162±3	147±5	154±13	
NGC 4321	53±15(0.12)	133±6	137±5	118±4	123±14	163±12	182±12	189±5	188±5	178±7	184±8	207±7	195
NGC 4605	11±2(0.13)	37±2	60±1	60±3	76±3	89±3							
NGC 4682	4±22(0.09)	63±12	90	108±4	122	114±9	141±8	139±10	149±6	160±2	170±4	170±4	176±4
NGC 7541	...	165±1	173±1	174	157±2	155±7	152±3	160±3	168±6	168±5	190±6	191±4	211±4
NGC 7664	...	...	137	138	148±5	151±3	157±3	174±3	186±2	188±6	193±3	189±6	183±4
IC 467	5±9(0.05)	37±5	55±6	72±4	82±4	96±6	106±5	115±6	125±2	127±4	122±2	129±4	162
UGC 2885	...	...	208	297±42	301	...	...	269±2	260±4	252	257±7	278±7	260
UGC 3691	17±(0.06)	24±8	33±7	39±5	55±2	78±5	94±2	91±3	102±4	105	115±12	116±4	133±2